^{13}C signatures of aerosol organic and elemental carbon from major combustion sources in China compared to worldwide estimates

Yao, Peng; Huang, Ru Jin; Ni, Haiyan; Kairys, Norbertas; Yang, Lu; Meijer, Harro A. J.; Dusek, Ulrike

Published in:
Science of the Total Environment

DOI:
10.1016/j.scitotenv.2021.151284

Science of the Total Environment 810 (2022) 151284

Contents lists available at ScienceDirect

Science of the Total Environment

journal homepage: www.elsevier.com/locate/scitotenv

^{13}C signatures of aerosol organic and elemental carbon from major combustion sources in China compared to worldwide estimates

Peng Yao [b], Ru-Jin Huang [a,*], Haiyan Ni [a,b], Norbertas Kairys [b], Lu Yang [a], Harro A.J. Meijer [b], Ulrike Dusek [b,*]

[a] State Key Laboratory of Loess and Quaternary Geology, Center for Excellence in Quaternary Science and Global Change, Key Laboratory of Aerosol Chemistry & Physics, Institute of Earth Environment, Chinese Academy of Sciences, Xi'an 710061, China
[b] Centre for Isotope Research (CIO), Energy and Sustainability Research Institute Groningen (ESRIG), University of Groningen, Groningen, 9747AG, the Netherlands

HIGHLIGHTS

- ^{13}C source signatures of EC and OC determined by thermal-optical method.
- Composite ^{13}C source signatures of EC with uncertainties and application conditions.
- A comprehensive literature review of ^{13}C source signatures.
- Distinct regional variation of ^{13}C signatures of crude oil and traffic EC.
- For the flaming combustion of C4 plants, OC can be strongly depleted in ^{13}C.

GRAPHICAL ABSTRACT

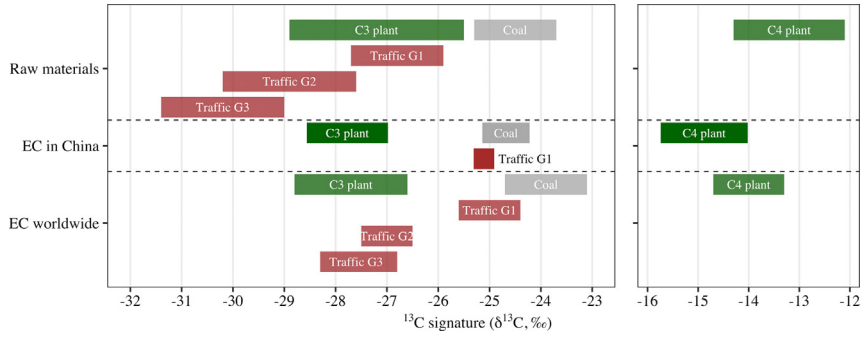

ARTICLE INFO

Article history:
Received 7 September 2021
Received in revised form 19 October 2021
Accepted 23 October 2021
Available online 2 November 2021

Editor: Pingqing Fu

Keywords:
Elemental carbon
^{13}C signature
Thermal-optical method
Source apportionment

ABSTRACT

Carbon isotope signatures are used to gain insight into sources and atmospheric processing of carbonaceous aerosols. Since elemental carbon (EC) is chemically stable, it is possible to apportion the main sources of EC (C3/C4 plant burning, coal combustion, and traffic emissions) using a dual ^{14}C-^{13}C isotope approach. The dual-isotope source apportionment crucially relies on accurate knowledge of ^{13}C source signatures, which are seldom measured for EC. In this work, we present ^{13}C signatures of organic carbon (OC) and EC for relevant sources in China. EC was isolated for ^{13}C analysis based on the OC/EC split point of a thermal-optical method (EUSAAR_2 protocol). A series of sensitivity studies were conducted to investigate the EC separation and the relationship of the thermal-optical method to other EC isolation methods. Our results show that, first, the ^{13}C signatures of raw materials and EC related to traffic emissions can be separated into three groups according to geographical location. Second, the ^{13}C signature of OC emitted by the flaming combustion of C4 plants is strongly depleted in ^{13}C compared to the source materials, and therefore EC is a better tracer for this source than total carbon (TC). A comprehensive literature review of ^{13}C source signatures (of raw materials, of TC, and of EC isolated using a variety of thermal methods) was conducted. Accordingly, we recommend composite ^{13}C source signatures of EC with uncertainties and detailed application conditions. Using these source signatures of EC in an example dual-isotope source apportionment study shows an improvement in precision. In addition, ^{13}C signatures of OC were measured at three different desorption temperatures roughly corresponding to semi-volatile, low-volatile, and non-volatile OC fractions. Each source category shows a characteristic trend of ^{13}C signatures with desorption temperature, which is likely related to different OC formation processes during combustion.

* Corresponding authors.
E-mail addresses: rujin.huang@ieecas.cn (R.-J. Huang), u.dusek@rug.nl (U. Dusek).

https://doi.org/10.1016/j.scitotenv.2021.151284
0048-9697/

1. Introduction

1.1. Carbonaceous aerosols and dual-isotope source apportionment

Carbonaceous aerosol is a major constituent of atmospheric particulate matter (Pöschl, 2005). Total carbon (TC) refers to the amount of carbon contained in carbonaceous aerosols (except for inorganic carbon) and can be further separated into organic carbon (OC) and elemental carbon (EC). EC is strongly light-absorbing and contributes significantly to the absorption of solar radiation by atmospheric aerosols (Ramanathan and Carmichael, 2008; Bond et al., 2013). OC contains a wide variety of organic compounds, which play a significant role in air pollution and radiative forcing of climate (Chung et al., 2012; Laskin et al., 2015). Quantifying the contribution of various pollution sources to OC and EC concentrations is therefore crucial for a better understanding of air pollution and global climate change.

Source apportionment is an approach to determine aerosol sources and their contribution to ambient aerosol concentrations. Different tracers, such as elements (Moreno et al., 2013), ions (Zhang et al., 2017), isotopes (Andersson et al., 2015; Ni et al., 2018; Masalaite et al., 2018), and specific organic compounds (Fu et al., 2012) are used in source apportionment. Radiocarbon (^{14}C) can be used as a tracer to distinguish between fossil and non-fossil sources. ^{14}C analysis has been used widely, e.g., (Szidat et al., 2004a; Gustafsson et al., 2009; Heal, 2014; Dusek et al., 2017) for source apportionment, and applied to carbon fractions such as OC (Dusek et al., 2013), EC (Heal et al., 2011), water-soluble carbon (WSOC) (Morera-Gómez et al., 2021), and more volatile OC (mvOC) (Ni et al., 2019a). In addition, ^{13}C source signatures have been found to differ for coal burning and traffic emissions, as well as for C3 and C4 plant burning. Therefore, ^{13}C and ^{14}C can be combined to achieve detailed insight into the sources. In regions where extensive coal burning and traffic emissions have an influence on air quality, a combination of ^{13}C and ^{14}C analysis in OC and EC is very promising to resolve contributions of the major sources, e.g., (Andersson et al., 2015; Fang et al., 2018; Ni et al., 2018).

There are two difficulties in using ^{13}C signatures of OC or TC for accurate source apportionment. First, a large part of secondary organic aerosol (SOA) originates from biogenic precursor emissions (Hallquist et al., 2009; Bianchi et al., 2019), with uncertain ^{13}C signatures. Second, organic aerosols can be aged in the atmosphere through photochemical processes, which leads to volatilization of part of the OC. The remaining OC tends to be gradually enriched in ^{13}C due to isotope fractionation (Killelea et al., 2008; Pavuluri and Kawamura, 2012).

In contrast, EC is chemically inert, so the ^{13}C value of EC is not strongly affected by aerosol transport, aging, photochemical reactions, and other processes in the atmosphere, and retains the original source information. Moreover, EC forms only in combustion and pyrolysis. Biomass burning, coal combustion, and traffic emissions are the main sources of EC. With limited sources and different ^{13}C signatures for biomass burning (C3 and C4 plants), coal combustion and traffic emissions, ^{13}C analysis of EC allows dual-isotope source apportionment using ^{13}C and ^{14}C (Andersson et al., 2015).

1.2. ^{13}C source signatures of raw materials

The ^{13}C signature is usually reported as $\delta^{13}C$, which is calculated as the relative deviation of the $^{13}C/^{12}C$ ratio (R^{13}) of the sample from the international primary standard Vienna Pee Dee Belemnite (VPDB):

$$\delta^{13}C = \frac{R^{13}_{Sample}}{R^{13}_{VPDB}} - 1, \quad (1)$$

usually reported in ‰. To achieve accurate dual-isotope source apportionment, reliable ^{13}C source signatures are increasingly important. The $\delta^{13}C$ value of the emitted aerosol depends on the fuel that is combusted. Many studies have already investigated the ^{13}C signatures of relevant raw materials. The ^{13}C signatures of coals from all over the world are summarized in Table S1. The ^{13}C signatures of coal do not vary strongly among different regions of the world (Mastalerz and Schimmelmann, 2002; Suto and Kawashima, 2016) and the worldwide average can be summarized as $-24.5‰ \pm 0.8‰$. Coal originated from prehistoric plants (mainly C3), and isotope fractionation during the transformation process resulted in differences in ^{13}C signatures between coal and the original biomass. The ^{13}C signatures of C3 and C4 plants from all over the world are shown in Tables S3 and S4. The difference in $\delta^{13}C$ between C3 and C4 plants is caused by different carbon fixation mechanisms. Most plant species on earth are C3 plants, such as most trees and grasses, rice, wheat, cotton, and soybeans. Common C4 plants include maize, sugarcane, and savanna grasses. There are many studies investigating the ^{13}C signatures of different types of biomass, and some of them analyzed a considerable number of samples in a specific area or worldwide, e.g. 1000 species worldwide (O'Leary, 1988), 478 species in China (Ren and Yu, 2011). These studies have shown that the ^{13}C signatures of global C3 and C4 plants follow approximately a unimodal normal distribution. Summarizing Tables S3 and S4, the worldwide averages are $-27.2‰ \pm 1.7‰$ for C3 plants and $-13.2‰ \pm 1.1‰$ for C4 plants. These two values are very similar to previous estimates in the literature, including worldwide averages of C3 plants (−27‰) and C4 plants (−13‰) of 1000 species (O'Leary, 1988), an average of C3 plants in China ($-27.10‰ \pm 1.70‰$) with 478 species (Ren and Yu, 2011), and an average of C3 foliar in China ($-27.23‰ \pm 1.54‰$) with 141 species (Zheng and Shangguan, 2007). Therefore, the worldwide averages in this study should be applicable to most areas including China. In addition, the ^{13}C signature of biomass can be influenced by geographical differences (essentially climatic difference, including rainfall gradient, light, temperature…) (Farquhar and Richards, 1984; Weiguo et al., 2005; de Bello et al., 2009; Yang et al., 2012) and the regional species (Farquhar et al., 1982; Ren and Yu, 2011), and this may be important for more regionally applicable values.

The ^{13}C signatures of crude oil from all over the world can be found in Table S2. The composition of oils varies with geographic regions, and the ^{13}C signatures of crude oil are actually determined by the geological periods of their formation (Andrusevich et al., 1998; Maslen et al., 2011). In addition, the microbial degradation before the formation of crude oil can also influence the ^{13}C signature (Huang et al., 2003). The ^{13}C signatures of crude oil in Table S2 are summarized and separated into groups based on statistical and geographical distributions in Fig. 6, and more discussion can be found in Section 4.

1.3. ^{13}C signatures of combustion products

Previous studies showed that the isotopic composition of combustion products can differ from the isotopic composition of the fuels (Bird and Ascough, 2012; and references therein). Studies include gaseous emissions (e.g. CO_2, CH_4) (Widory, 2006; Yang et al., 2011; Schumacher et al., 2011), particulate emissions (Turekian et al., 1998; Das et al., 2010; Garbaras et al., 2015; Aguilera and Whigham, 2018), or charcoal and ash (Turney et al., 2006; Malghani et al., 2013). OC and EC, which are parts of particulate emissions, form in different ways, and therefore the ^{13}C signatures of OC and EC from the same combustion source can be different (Yao et al., 2021). As a consequence, the ^{13}C signatures of raw materials and other specific combustion products, are not directly applicable as substitutes for ^{13}C source signatures of EC, and it is important to characterize the ^{13}C source signatures of OC and EC independently.

Compared to ^{13}C signatures of raw materials, very few studies characterize the ^{13}C signatures of OC and EC emitted by combustion. The majority of these studies use thermal methods to isolate OC and EC for ^{13}C analysis. Usually, OC is first desorbed in an inert atmosphere. The remaining fraction is combusted in an oxidizing atmosphere and classified as EC for ^{13}C analysis. However, during the first inert heating step, some

organic compounds will pyrolyze and form pyrolyzed organic carbon (pOC), which can only be combusted in an oxidizing atmosphere together with EC. pOC is therefore a common artifact of OC/EC separation methods (Szidat et al., 2004b; Zhang et al., 2012; Dusek et al., 2014) and, if it is analyzed together with EC, can skew the isotopic signatures of EC. There are also several studies combusting OC in an oxidizing atmosphere at low temperature to minimize pyrolysis and remove pOC and then combusting the remaining part at high temperature as EC for ^{13}C analysis, e.g., the CTO-375 method (Gustafsson et al., 1997). However, in these methods, some part of EC is already combusted in the low temperature oxygen step due to the long duration. To date, no ^{13}C source signatures of EC have been obtained by thermal-optical methods, such as EUSAAR_2 (Cavalli et al., 2010), IMPROVE (Chow et al., 2001), or NIOSH 5040 (Birch and Cary, 1996), which use an optical compensation to correct for the contribution of light-absorbing pOC to EC.

It is important to determine reliable ^{13}C source signatures of EC before applying them to source apportionment. A previous study shows that pOC formation and EC loss both can have an impact on the ^{13}C values of EC in aerosol samples and source samples (Yao et al., 2021). By reducing the influence of pOC, thermal-optical methods are expected to achieve more reliable ^{13}C source signatures of EC. In addition, the differences between ^{13}C source signatures of raw materials, TC, OC, and EC have not been systematically investigated for a wider range of sources.

1.4. General introduction of experiments

In this study, we test the application of the thermal-optical method to determine ^{13}C source signatures of EC, including typical coal/biomass burning samples and traffic (tunnel) samples from China. Additionally, we report ^{13}C source signatures of OC desorbed in three temperature steps. A sensitivity study of pOC/EC separation investigates, how sensitive the ^{13}C signatures of EC are to various approaches to EC isolation. Combining the results obtained by this study with a literature survey, we recommend composite ^{13}C source signatures of EC with uncertainties and detailed application conditions. Finally, we test the new source signatures for dual-isotope source apportionment of ambient samples in China and compare to previous studies.

2. Materials and methods

2.1. Source samples

Some representative biomass samples from major crop-producing regions in China were collected for combustion experiments, including wheat straw (C3 plant) from Anhui Province, soybean straw (C3 plant), and poplar wood (C3 plant) from Shaanxi Province, and corn stalk (C4 plant) from Hebei Province. Some coal samples from different mine regions throughout China were collected for combustion experiments, including anthracite (A) coal from Shaanxi Province, and bituminous (B) coals from Shaanxi Province, Ningxia Province, Shanxi Province, and Inner Mongolia. According to the standard GB/T 5751–2009 (GB/T 5751–2009), anthracite coal refers to coals with volatile matter content (V_{daf}, dry ash-free) less than or equal to 10.0%, and bituminous coal is the coal with V_{daf} between 10.0% and 37.0%.

A typical Chinese household coal stove was used for combustion, measuring 51 cm height, 31 cm diameter, and 12 cm inner diameter. The air inlet hole is 6 cm in diameter and located near the bottom of the stove. The combustion experiments were conducted with 200–300 g samples each time. The combustion exhaust was drawn through a diluter with dilution ratios of ~5 and collected with a $PM_{2.5}$ impactor sampler (Airmetrics, OR, USA) at a flow rate of 5 L/min for 10–20 min duration on quartz filters (Φ 47 mm, Whatman, QM-A, Clifton, NJ, USA). The effective diameter of the sampler was 38 mm, and the particle size selected was $PM_{2.5}$. The quartz filters were precleaned at 780 °C for 3 h to remove potential absorbed volatile organics. After sampling, the filters were packed in prebaked aluminum foil (450 °C, 3 h), sealed in polyethylene bags, and stored in the freezer at −18 °C. The combustion information and carbon fractions are shown in Table S6.

Traffic samples were collected from Wucun Tunnel and Xianyueshan Tunnel in Xiamen City, China. Sampling was conducted in the entrance and the exit of the tunnels with a high-volume sampler (TE-6070 MFC, Tisch Inc., Cleveland, OH, USA) at 1 m^3/min and 4 h duration (Morning 7:00–11:00, Afternoon 12:00–16:00, Evening 17:00–21:00, local standard time, LST) from 17 September to 22 September 2014. $PM_{2.5}$ samples were collected on precleaned (780 °C, 3 h) quartz fibber filters (20.3 cm × 25.4 cm, Whatman QM-A, Clifton, NJ, USA). A video camera was placed at the exit to record the passing vehicles during the sampling periods. The sampling information and carbon fractions, as well as meteorological parameters and vehicle information during the sampling periods are shown in Tables S7a–b.

2.2. OC/EC separation and ^{13}C analysis

The ^{13}C values of TC, OC, and EC ($\delta^{13}C_{TC}$, $\delta^{13}C_{OC}$, $\delta^{13}C_{EC}$) were measured on the filters containing biomass burning, coal combustion, and traffic emissions. A newly developed system that couples a thermal-optical analyzer (TOA, Sunset Laboratory Inc.) to an isotope ratio mass spectrometer (IRMS) was used for ^{13}C analysis (Yao et al., 2021). OC and EC were first separated in the TOA and combusted into CO_2. Then the CO_2 was automatically collected, purified, and injected into IRMS for ^{13}C analysis. The system works at normal pressure for combustion, and nearly vacuum for CO_2 capture.

Fig. 1 gives an overview of the carbon fractions of the thermal protocols used in this study. TC and EC were sequentially collected for ^{13}C analysis based on the EUSAAR_2 protocol. On a first filter piece, all CO_2 evolved during the EUSAAR_2 protocol (except the calibration gas, methane) was captured for $\delta^{13}C_{TC}$ analysis. At the same time, the OC/EC split was determined based on the laser transmission signal and later used for the isolation of EC. On a second filter piece, only the CO_2 evolved after the split time (except the calibration gas, methane) was captured for $\delta^{13}C_{EC}$ analysis. Repeated analyses of the same filter sample show that small variations of the split time have little impact on $\delta^{13}C_{EC}$ results. To avoid ambiguity, the abbreviation OC in the following description refers specifically to total OC as analyzed by the EUSAAR_2 protocol, which consists of desorbed OC (dOC) and pOC. $\delta^{13}C_{OC}$ was calculated from the isotopic mass balance, from measured values of $\delta^{13}C_{TC}$ and $\delta^{13}C_{EC}$ (Eq. (2)). Uncertainties were propagated using a Monte Carlo method.

$$\delta^{13}C_{OC} = \left(TC \times \delta^{13}C_{TC} - EC \times \delta^{13}C_{EC}\right)/OC \quad (2)$$

Different fractions of OC were desorbed for subsequent ^{13}C analysis under inert carrier gas flow (Helium) using the OC_3step protocol, which consists of three temperature steps (200 °C, 350 °C, and 650 °C) for 5 min each, as described in (Zenker et al., 2020). Since more volatile organic compounds tend to evaporate at lower temperatures, this separates OC approximately into compound classes with lower and higher

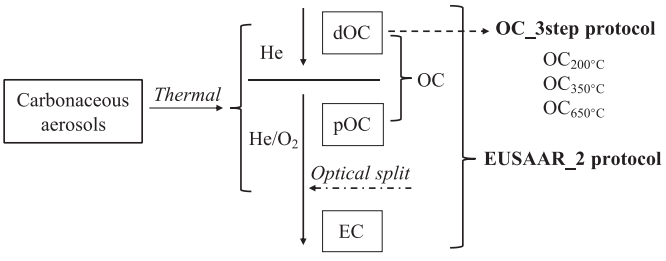

Fig. 1. OC/EC separation protocols used in this study. dOC and pOC refer to desorbed part and pyrolyzed part of total OC.

volatilities. As the maximum desorption temperature used (650 °C) in the OC_3step protocol is equal to that of the EUSAAR_2 protocol, the sum of the three fractions (dOC_3step) corresponds to dOC. A comparison between $\delta^{13}C_{OC}$ and $\delta^{13}C_{dOC\_3step}$ can be found in Fig. S2, where differences are caused by the influence of pOC.

Carbonates usually decompose when the temperature rises to 600 °C or higher (Gallagher and Johnson, 1973), and the decomposition rate increases with temperature. It means that potential carbonates in aerosol samples, especially in tunnel samples with road dust, may decompose during analysis and influence the ^{13}C value. Since the last step in He of EUSAAR_2 protocol is 650 °C, carbonates will decompose in this step if present, and the $\delta^{13}C_{EC}$ in this study should not be affected. To investigate if carbonate influence the traffic $\delta^{13}C_{OC}$, we decreased the 650 °C step of OC_3step protocol to 550 °C for comparison.

The $\delta^{13}C$ values were calibrated based on two local reference materials CAN (isotopically enriched caffeine, $\delta^{13}C = 0.61‰ \pm 0.15‰$), CAF (caffeine, $\delta^{13}C = -38.20‰ \pm 0.15‰$) with a two-point linear calibration. The international reference material LVal (L-Valine, USGS73, $\delta^{13}C = -24.03‰ \pm 0.04‰$) was used as quality control (Schimmelmann et al., 2016). The standard reagents were first dissolved in deionized water (around 3 μg/μL), and then the solutions were loaded on a quartz filter, dried at 110 °C, and converted into CO_2 in the TOA for ^{13}C analysis at 650 °C under He flow, similar to the aerosol samples. The ^{17}O correction of Craig (Craig, 1957) was used in our IRMS software, but since reference materials have been determined using the ^{17}O correction method of Brand (Brand et al., 2010), the calibrated results agree with the latter correction method within <0.01‰. The CAN and CAF standards were measured at least once per day, and the LVal quality control standard was analyzed at least twice per day. The two-point linear calibration was calculated approximately every week using all $\delta^{13}C$ values of CAN and CAF measured during that week for the linear fit. The $\delta^{13}C$ value of LVal was used for evaluation of the uncertainty, the bias, and a potential drift over the day and over long time periods. The corrected LVal values from June 2019 to January 2020 are shown in Fig. S3, and the standard deviation (0.19‰) is in an acceptable range.

2.3. Ambient aerosol samples and dual-isotope source apportionment

The ^{13}C and ^{14}C raw data of ambient aerosol samples were collected from a previous study (Ni et al., 2020) and were used to re-evaluate the source apportionment with the new source signatures. The sampling was conducted at the building rooftop of the Institute of Earth Environment, Chinese Academy of Sciences, Xi'an, China (34.23°N, 108.88°E, 10 m above the ground). $PM_{2.5}$ samples were collected on pre-combusted quartz filters (1.0 m^3/min, TE-6070 MFC, Tisch Inc., Cleveland, OH, USA) with a high-volume aerosol sampler for 12 h duration each (daytime: 8:00 a.m. to 8:00 p.m.; nighttime: 8:00 p.m. to 8:00 a.m.; local standard time, LST) from 1 January 2017 to 10 January 2017. A source apportionment considering four sources was applied to these clean/haze aerosol samples. The dual-isotope source apportionment in EC was conducted with the following equations, considering 4 sources, namely, fossil (coal and traffic) and non-fossil (C3 and C4 plants).

$$EC = EC_{coal} + EC_{traffic} + EC_{C3} + EC_{C4} \quad (3)$$

$$EC \times F^{14}C_{EC} = (EC_{coal} + EC_{traffic}) \times F^{14}C_{fossil} + (EC_{C3} + EC_{C4}) \times F^{14}C_{non-fossil} \quad (4)$$

$$EC \times \delta^{13}C_{EC} = EC_{coal} \times \delta^{13}C_{coal} + EC_{traffic} \times \delta^{13}C_{traffic} + EC_{C3} \times \delta^{13}C_{C3} + EC_{C4} \times \delta^{13}C_{C4} \quad (5)$$

The *simmr* package in R software was used for the source apportionment, in which Bayesian Markov chain Monte Carlo (MCMC) was used to propagate uncertainties (Parnell et al., 2010; Andersson et al., 2015). The C4 source was excluded in the equations for 3-source apportionment. The emissions from fossil sources are ^{14}C-free, whereas non-fossil emissions contain the contemporary ^{14}C content ($F^{14}C_{fossil} = 0$, $F^{14}C_{non\text{-}fossil} = 1.10 \pm 0.05$) (Lewis et al., 2004; Mohn et al., 2008; Palstra and Meijer, 2014; Ni et al., 2019b). The ^{13}C source signatures of EC are determined by this study and can be different for different geophysical areas.

3. Results

3.1. Typical ^{13}C source signatures of EC in China

The $\delta^{13}C$ values of TC, OC, and EC of biomass burning, coal combustion, and traffic emissions are shown in Table 1. The $\delta^{13}C$ values of TC, OC, and EC all follow the same order: C4 plant > coal > traffic > C3 plant, despite the small differences in $\delta^{13}C$ between TC, OC, and EC within each source category. For C3 plant burning, differences between $\delta^{13}C_{EC}$ and $\delta^{13}C_{TC}$ vary among the species of plants, with EC depleted in ^{13}C for wood ($\Delta^{13}C = -0.67‰$; where $\Delta^{13}C$ refers to the difference between the $\delta^{13}C$ values of EC and TC), EC enriched in ^{13}C for wheat straw ($\Delta^{13}C = 0.89‰$), and no obvious difference for soybean straw. The $\delta^{13}C_{EC}$ values for C3 plant burning also vary by region (Fig. 2), but it is not clear whether the variation originates from geographical differences (Farquhar and Richards, 1984; Weiguo et al., 2005; Yang et al., 2012) and/or species (Farquhar et al., 1982; Ren and Yu, 2011). For corn stalk, the main C4 plant in China, $\delta^{13}C_{EC}$ is lower than $\delta^{13}C_{TC}$, by 3.04‰ for flaming and by 0.36‰ for smoldering combustion, respectively. This is due to the strong enrichment in ^{13}C of OC produced during flaming combustion (Table 1). $\delta^{13}C_{EC}$ values are also different for flaming (−15.38‰; OC/EC ≈ 5) and smoldering (−13.89‰; OC/EC ≈ 14) combustion conditions, but the difference is much smaller than the one of $\delta^{13}C_{OC}$.

For coal combustion samples, $\delta^{13}C_{TC}$ values are similar to $\delta^{13}C_{OC}$ values, but slightly lower than $\delta^{13}C_{EC}$ values. However, $\delta^{13}C$ values of OC, EC, and TC for all coals vary in a narrow range from −24.19‰ to −25.28‰. In Fig. 2, the ^{13}C signature of EC from coal combustion changes only slightly with the geophysical location of the major coal mine belts. Since these provinces provide the main coal supply in China, the average ^{13}C signatures of coal combustion should be applicable for most areas in China, except for some coastal cities (e.g., Xiamen) which import coal for industry and energy supply.

For traffic samples, EC is enriched in ^{13}C compared to TC, while OC is depleted. The standard deviation of $\delta^{13}C_{EC}$ values is smaller than 0.3‰, which shows that sampling dates and times exert small influence on $\delta^{13}C$. The $\delta^{13}C_{EC}$ values are also similar between the two tunnels, indicating that emissions from different vehicles (Table S7b) are well mixed in tunnels and provide a representative traffic ^{13}C signature of EC. Crude oil used in Xiamen, a coastal city in South China (Fig. 2), is mostly imported from the Middle East (customs data in Table S11). Therefore, the traffic ^{13}C signature of EC in Table 1 is representative for other locations using crude oil from the same producing area.

Due to the difference between $\delta^{13}C_{EC}$ and $\delta^{13}C_{TC}$ (e.g., maximum 3.04‰ between flaming and smoldering combustion of corn stalk), $\delta^{13}C_{TC}$ is not always suitable as a substitute or approximation of ^{13}C source signature of EC in source apportionment. On the other hand, repeated combustion experiments of the same raw material give reproducible results, which gives confidence that representative ^{13}C source signatures of EC, OC, and TC can be obtained by averaging over multiple combustion experiments.

On a regional scale, different species of coal or biomass may be combusted under various conditions. Building a localized database of ^{13}C source signatures of EC is important for accurate source apportionment. In addition, the $\delta^{13}C_{EC}$ values of coal and traffic emissions are sometimes similar (Fig. 2), but the mean values are actually different at 95% confidence level (Welch Two Sample *t*-test, $p = 0.0036$) and can still be applied to EC source apportionment.

Table 1
Typical ^{13}C source signatures of EC (biomass, coal, and tunnel) in China determined by the thermal-optical method.

Sample name/tunnel name	Combustion/location	N[b]	$\delta^{13}C_{TC}$ (‰)	SD[c]	$\delta^{13}C_{EC}$ (‰)	SD	$\delta^{13}C_{OC}$ (‰)[d]	Unc.
Soybean straw (C3)	Flaming	3	−28.13	0.23	−28.27	0.17	−28.11	0.25
Poplar wood (C3)	Flaming	2	−27.75		−28.42		−27.62	
Wheat straw (C3)	Smoldering then flaming	3	−27.73	0.20	−26.84	0.24	−27.78	0.23
Corn stalk (C4)	Flaming	2	−18.42		−15.38		−19.12	
	Smoldering	1	−14.25		−13.89		−14.27	
Shaanxi coal (B)[a]		3	−24.37	0.20	−24.22	0.29	−24.47	0.35
Ningxia coal (B)		3	−24.58	0.02	−24.19	0.07	−24.60	0.14
Shanxi coal (B)		3	−24.93	0.20	−24.94	0.36	−24.93	0.22
Inner Mongolia coal (B)		3	−25.28	0.16	−25.12	0.35	−25.28	0.16
Shaanxi coal (A)		3	−25.16	0.19	−24.92	0.20	−25.17	0.20
Wucun Tunnel	Entrance	4	−25.84	0.23	−25.06	0.09	−26.34	0.32
	Exit	4	−25.88	0.24	−24.89	0.07	−26.61	0.41
Xianyueshan Tunnel	Entrance	4	−25.88	0.26	−25.29	0.24	−26.28	0.36
	Exit	4	−25.79	0.23	−25.18	0.14	−26.47	0.45

[a] B refers to bituminous coal; A refers to anthracite coal.
[b] For combustion samples, N is the number of combustion experiments for each fuel type. For tunnel samples, N is the number of samples collected on different dates and time periods of the day.
[c] Each filter sample was analyzed once, and SD refers to the standard deviation of $\delta^{13}C$ values between the different combustion experiments, rather than repeated ^{13}C measurements on one filter sample. For samples combusted once or twice, the laboratory ^{13}C long-term measurement uncertainty of QC LVal (0.19‰) was used.
[d] The $\delta^{13}C_{OC}$ is calculated from $\delta^{13}C_{TC}$ and $\delta^{13}C_{EC}$ based on isotopic mass balance, and the uncertainty comes from error propagation.

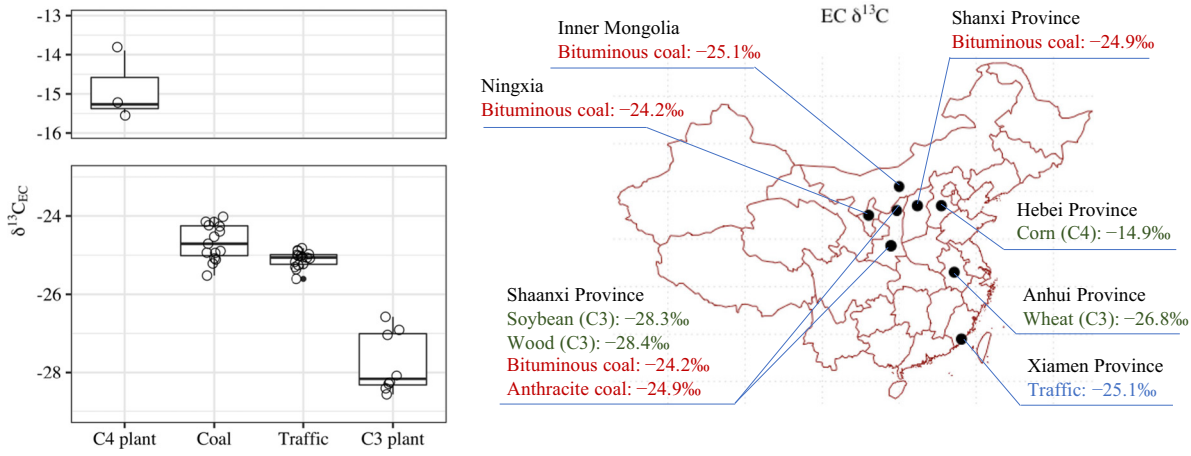

Fig. 2. The ^{13}C source signatures of EC emitted from various combustion sources in China and their geographic distribution.

3.2. ^{13}C source signatures of OC fractions desorbed at different temperatures

$\delta^{13}C$ of OC desorbed at different temperatures ($OC_{200°C}$, $OC_{350°C}$, and $OC_{650°C}$; $\delta^{13}C_{OC200}$, $\delta^{13}C_{OC350}$, $\delta^{13}C_{OC650}$) for primary sources can be interpreted as ^{13}C signatures of semi-volatile, low-volatile, and non-volatile primary combustion emissions, and are shown in Table 2 and Fig. 3. There are differences (significant at the 95% confidence level, unless otherwise mentioned) between $\delta^{13}C_{OC}$ values at different

Table 2
^{13}C source signatures of OC fractions desorbed at different temperatures.

Sample name/tunnel name	Combustion/location	N[b]	$\delta^{13}C_{OC200}$ (‰)	SD[c]	$\delta^{13}C_{OC350}$ (‰)	SD	$\delta^{13}C_{OC650}$ (‰)	SD
Soybean straw (C3)	Flaming	3	−27.15	0.34	−28.12	0.46	−28.28	0.52
Poplar wood (C3)	Flaming	2	−27.17		−28.02		−28.16	
Wheat straw (C3)	Smoldering then flaming	3	−26.69	0.41	−27.97	0.06	−27.45	0.26
Corn stalk (C4)	Flaming	2	−22.89		−18.67		−18.12	
	Smoldering	1	−14.68		−14.06		−13.38	
Shaanxi coal (B)[a]		3	−24.97	0.27	−24.07	0.25	−24.41	0.31
Ningxia coal (B)		3	−24.66	0.27	−23.93	0.32	−24.58	0.27
Shanxi coal (B)		3	−25.60	0.30	−24.70	0.36	−25.16	0.19
Inner Mongolia coal (B)		3	−25.81	0.33	−24.88	0.09	−25.50	0.24
Shaanxi coal (A)		3	−25.11	0.21	−24.48	0.35	−24.92	0.31
Wucun Tunnel	Entrance	4	−27.72	0.15	−26.46	0.32	−25.39	0.76
	Exit	4	−27.88	0.23	−26.78	0.28	−25.18	0.21
Xianyueshan Tunnel	Entrance	4	−27.73	0.25	−26.93	0.15	−25.00	0.13
	Exit	4	−28.02	0.18	−27.01	0.17	−24.65	0.13

[a] B refers to Bituminous coal; A refers to Anthracite coal.
[b] For combustion samples, N is the number of combustion experiments for each fuel type. For tunnel samples, N is the number of samples collected on different dates and time periods of the day.
[c] Each filter sample was analyzed once, and SD refers to the standard deviation of $\delta^{13}C$ between the different combustion experiments, rather than repeated ^{13}C measurements on one filter sample. For samples combusted once or twice, the laboratory ^{13}C long-term measurement uncertainty of QC LVal (0.19‰) was used.

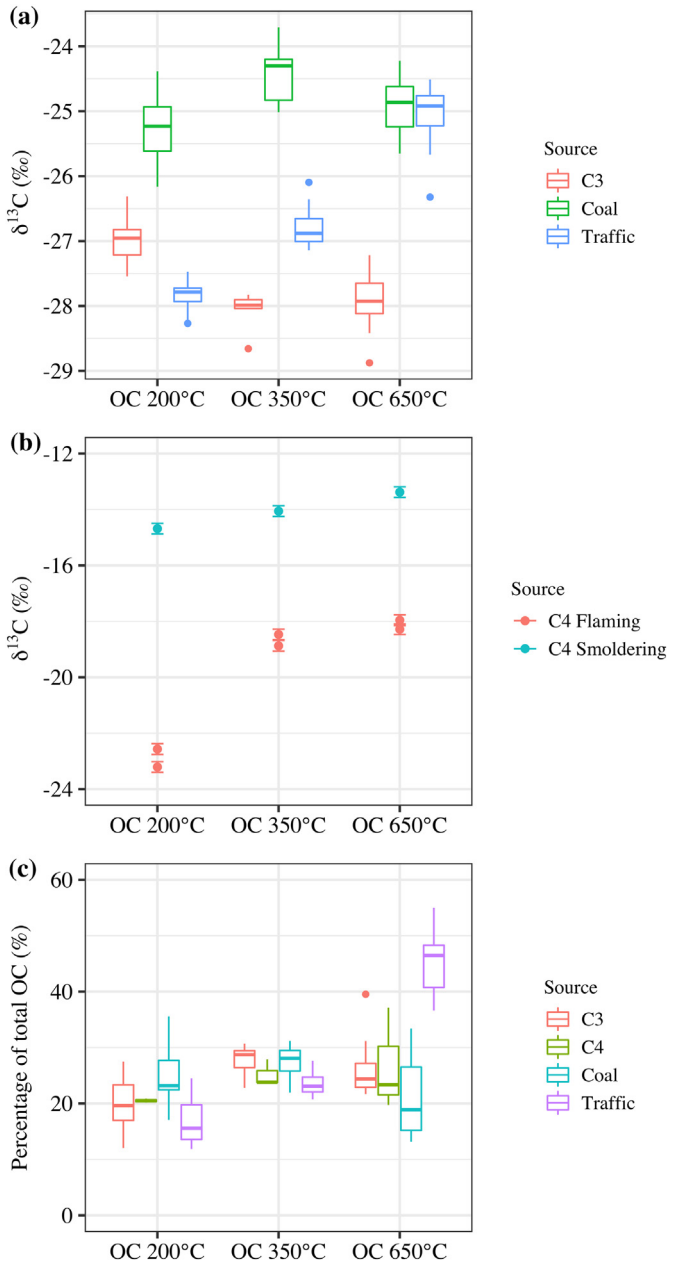

Fig. 3. (a) ^{13}C source signatures of OC desorbed at different temperatures (200 °C, 350 °C, 650 °C) for C3 plant and coal burning, as well as traffic emissions. (b) ^{13}C signatures of OC desorbed at different temperatures for flaming and smoldering combustion of C4 plant. (c) The mass percentage of OC desorbed at different temperature steps (200 °C, 350 °C, 650 °C; OC_3step protocol) in the total OC (EUSAAR_2 protocol). The mass percentages do not add up to 100%, because of pOC (accounting for 10%–40% of total OC mass, Tables S6–S7).

temperature steps for the same fuel, as well as between different fuels at the same temperature step. In Fig. 3a, $\delta^{13}C_{OC200}$ values of C3 plant burning are around 1‰ higher than $\delta^{13}C_{OC350}$ and $\delta^{13}C_{OC650}$. This is different from a study of C3 plant (oak) burning in Italy, in which $\delta^{13}C_{OC650}$ is the highest (Zenker et al., 2020). It is not clear whether the burning conditions or the biomass species cause the difference. For coal combustion, the differences among $\delta^{13}C_{OC200}$, $\delta^{13}C_{OC350}$, and $\delta^{13}C_{OC650}$ are within 1‰, with the highest $\delta^{13}C$ value at 350 °C and the lowest at 200 °C. The opposite $\delta^{13}C$ trends of OC fractions between C3 plants and coal are a distinctive feature for these two combustion sources, which indicates a potential different OC formation mechanism and needs further investigation. Differences in the composition of various fuel components may be one possible explanation. Biomass contains different chemical fractions (e.g., cellulose, lipids) with distinct ^{13}C signatures, which can contribute to different OC volatility classes, but the coal is relatively more homogeneous.

Compared with C3 plant and coal burning, the traffic OC fractions vary significantly in ^{13}C (around 3‰, Fig. 3), and $\delta^{13}C$ increases with the increase of desorption temperature. The OC fractions desorbed at low temperatures ($\delta^{13}C_{OC200}$ average, −27.84‰ ± 0.22‰; $\delta^{13}C_{OC350}$, −26.80‰ ± 0.31‰, Table S9) are significantly depleted in ^{13}C with respect to EC (Fig. 2). Therefore, $\delta^{13}C_{TC}$ and $\delta^{13}C_{OC}$ may not well represent the approximation of traffic $\delta^{13}C_{EC}$. The traffic $\delta^{13}C_{OC200}$ and $\delta^{13}C_{OC350}$ are also similar to bus emissions and a tunnel studies in Italy (Zenker et al., 2020), with differences <0.6‰. However, the tunnel $\delta^{13}C_{OC650}$ measured in Xiamen (−25.05‰ ± 0.47‰; this study) is different from the bus (−28.37‰ ± 0.60‰) and tunnel (−19.11‰ ± 0.42‰) values in Italy. The very high tunnel $\delta^{13}C_{OC650}$ in Italy is likely influenced by the carbonates from road dust, which are usually enriched in ^{13}C, e.g., street dust (−17.0‰ ± 0.1‰) and volcanic dust (−22.7‰ ± 1.4‰) in Mexico (López-Veneroni, 2009), dust storms (−5.0‰ to −9.7‰) in China (Chen et al., 2015), curb stone dust (−13.45‰) in China (Guo et al., 2016). Carbonates tend to decompose at temperatures higher than 600 °C (Gallagher and Johnson, 1973), so we decreased the third step from 650 °C to 550 °C to eliminate the influence of road dust. The traffic $\delta^{13}C_{OC550}$ (−25.56‰) is not very different from $\delta^{13}C_{OC650}$, indicating negligible influence of road dust in our case. The higher $\delta^{13}C_{OC650}$ value in the bus exhaust study in Italy is therefore likely caused by different vehicle types or fuel additives.

For C4 plant burning (corn stalk), the $\delta^{13}C$ values of OC fractions are all lower than $\delta^{13}C_{EC}$, and vary greatly with the combustion conditions (Fig. 3b). OC fractions emitted under flaming conditions are significantly depleted in ^{13}C compared to OC fractions produced under smoldering conditions, with a difference $\Delta^{13}C$ of −8.21‰ for $OC_{200°C}$, −4.61‰ for $OC_{350°C}$, and −4.74‰ for $OC_{650°C}$ (Table S9). However, the difference in $\delta^{13}C_{EC}$ between flaming and smoldering combustion is relatively smaller (−15.38‰ vs −13.89‰, a difference of $\Delta^{13}C = -1.49$‰; Table 1). With these much more ^{13}C depleted OC fractions in flaming conditions, the ^{13}C signature of EC can be strongly influenced by mixing with pOC if not well separated.

Overall, the results show that different temperature fractions of OC are not homogeneous in isotope composition. In principle, the different $\delta^{13}C_{OC}$ values for higher and lower desorption temperatures show promise for OC source apportionment. However, since ambient organic aerosol (OA) is not chemically stable, source apportionment is complicated by biogenic SOA formation, OA aging, and accompanying isotope fractionation. These should be further studied before quantitative OC source analysis using ^{13}C signatures is possible.

Fig. 3c shows the mass percentage of OC desorbed at different temperature steps (200 °C, 350 °C, 650 °C; OC_3step protocol) with respect to the total OC (EUSAAR_2 protocol). For the burning of C3 plants, C4 plants and coal, the mass fractions of OC were similar (17%–28%, Fig. 3c and Table S10) among different desorption temperatures, different fuel types, and combustion experiments, even for flaming and smoldering combustion. However, for traffic emissions, $OC_{650°C}$ is the largest fraction and accounts for 45% of OC. In general, the mass fractions do not necessarily add up to 100%, because part of the OC is not desobed but forms pOC instead. This pOC accounts for 26%–28% of the total OC for biomass (C3 and C4 plants) and coal combustion, and around 15% for traffic emissions. Regarding ^{13}C analysis, pOC formation can cause a difference in $\delta^{13}C$ between desorbed OC and total OC, if $\delta^{13}C$ of pOC is significantly different from the desorbed part. As shown in Fig. S2, the differences between $\delta^{13}C_{OC}$ and $\delta^{13}C_{dOC\_3step}$ are noticeable for traffic emissions, but small for other sources. This means that traffic $\delta^{13}C_{pOC}$ is different from $\delta^{13}C_{OC}$ (actually close to $\delta^{13}C_{EC}$), but $\delta^{13}C_{pOC}$ of other sources is close to $\delta^{13}C_{OC}$. These characteristics are explored further in the following sensitivity studies.

3.3. Sensitivity studies of pOC/EC separation

Currently, $\delta^{13}C_{EC}$ values are analyzed by various methods in the literature, which capture different fractions. The EC fractions are potentially mixed with pOC, which is an artifact of the analysis method, produced from OC during inert heating steps. For methods that use a laser split point to isolate EC from pOC, the timing of the split point can vary, depending on e.g., the thermal protocol, or the filter loading (Zenker et al., 2017). To investigate if variations in the split point have a strong influence on $\delta^{13}C_{EC}$, we capture the carbon remaining on the filter at various times before and after the split point for ^{13}C analysis. This sensitivity study is summarized in Fig. 4. The x-axis shows the analysis time in the EUSAAR_2 protocol. The vertical dash-dot line indicates the time, where the carrier gas switched from He to He/O_2. At this point all the desorbed OC has been removed in the He phase, while pOC and EC remain on the filter. With increasing analysis time in the He/O_2 phase, more and more carbon is combusted. Since pOC is thermally less stable than the majority of EC, which is formed at high combustion temperatures, it is usually removed at earlier analysis times in the He/O_2 phase. The vertical bars in the lower panel of the figure indicate the carbon fraction that remains on the filter as a function of analysis time. This remaining carbon fraction (RC) was collected for ^{13}C measurement and the respective $\delta^{13}C$ values are shown in the upper panel of Fig. 4. As the analysis time increases, RC represents the transition from pOC + EC (the first point in Fig. 4 at the start of the He/O_2 phase) to our best estimate of EC (at the split point), to more refractory EC fractions (collected after the split point).

Fig. 4a shows the change of $\delta^{13}C_{RC}$ with increasing analysis time for emissions from C3 plant burning. The $\delta^{13}C_{RC}$ values of soybean and wheat both increase by 1‰ from the start of the He/O_2 phase to the last data point. Since $\delta^{13}C_{pOC+EC}$ is lower than $\delta^{13}C_{EC}$ isolated after the split point, this suggests that $\delta^{13}C_{pOC}$ is lower than $\delta^{13}C_{EC}$. If pOC is not well separated from EC, this could lead to biased lower $\delta^{13}C_{EC}$. However, since the differences between pOC + EC and EC are on the order of 0.5‰, analyzing a fraction of pOC together with EC should therefore only have a moderate influence on ^{13}C source signatures.

Fig. 4b shows a similar analysis for samples from C4 plant burning. The $\delta^{13}C_{RC}$ values are much lower for samples collected under flaming than under smoldering conditions, especially $\delta^{13}C_{pOC+EC}$ (−16.40‰ for Flaming1, −17.25‰ for Flaming2, −14.53‰ for Smoldering). On the other hand, the $\delta^{13}C_{RC}$ values increase by 1.1‰ (Flaming1), 1.8‰ (Flaming2), and 0.6‰ (Smoldering) from pOC + EC (at the start of the analysis) to EC remaining at the split point. Under flaming combustion conditions, OC (and as a consequence pOC), are strongly depleted in ^{13}C compared to the typical raw plant material (Fig. 3). Therefore, the strong increasing trend in $\delta^{13}C_{RC}$ from the start of the He/O_2 phase to the split point is consistent with the preferential removal of pOC before the split point. In contrast, under smoldering combustion conditions $\delta^{13}C_{pOC+EC}$ and $\delta^{13}C_{EC}$ are similar, consistent with $\delta^{13}C_{OC}$. This suggests that pOC and EC have similar $\delta^{13}C$ values, and consequently $\delta^{13}C_{EC}$ is much less sensitive to the timing of the split point.

In Fig. 4c, the $\delta^{13}C_{RC}$ values of coal combustion samples are relatively stable (within 0.5‰) as pOC is gradually oxidized and finally less refractory EC is also combusted. The comparable $\delta^{13}C_{RC}$ values before and after the OC/EC split suggest that $\delta^{13}C_{EC}$ of coal combustion samples is not sensitive to the split time. Moreover, $\delta^{13}C_{pOC+EC}$ is comparable with $\delta^{13}C_{EC}$, suggesting that pOC has similar $\delta^{13}C$ value with EC. This is consistent with similar $\delta^{13}C_{OC}$ and $\delta^{13}C_{EC}$ in Table 1.

Compared to biomass (C3/C4) and coal burning (where pOC accounts for roughly 23% of TC), much lower pOC mass fractions (9% of TC) were found for tunnel traffic samples (Fig. 5) and the OC/EC split time is on average earlier. The $\delta^{13}C_{RC}$ values first increase and then decrease with analysis time for both entrance/exit and two different tunnels, and the $\delta^{13}C_{RC}$ at split time ($\delta^{13}C_{EC}$) is the highest. However, the differences are in the range of the measurement uncertainties and therefore not significant. This indicates that $\delta^{13}C$ values of pOC and EC are comparable and $\delta^{13}C_{EC}$ is not sensitive to the isolation protocol used. This is in contrast to the strong $\delta^{13}C$ variation among the OC fractions for traffic samples in Fig. 3a. Since $\delta^{13}C_{RC}$ values are similar before and after the split time, variations in the split time should not make much difference to the determination of traffic ^{13}C signature of EC.

In summary, for C3 plant burning, C4 plant burning under smoldering conditions, coal combustion, and traffic emissions, $\delta^{13}C_{RC}$ values do not change strongly with time around the OC/EC split (within 1‰ for C3 plants, 0.6‰ for C4 plant smoldering, 0.5‰ for coal, and 0.5‰ for traffic). This suggests that the $\delta^{13}C_{EC}$ values of these sources may not be strongly influenced by the isolation protocol of EC, for example by various degrees of pOC removal or uncertainties in OC/EC split point. Therefore, the ^{13}C signatures of EC determined by various methods (e.g., thermal methods without optical correction, the thermal methods in an oxidizing atmosphere) should be comparable for the above sources. However, the $\delta^{13}C_{RC}$ values of C4 plant flaming change strongly (1.1‰ and 1.8‰ in our case), which means that pOC could influence the ^{13}C signature of EC from flaming combustion of C4 plants, if not separated from EC.

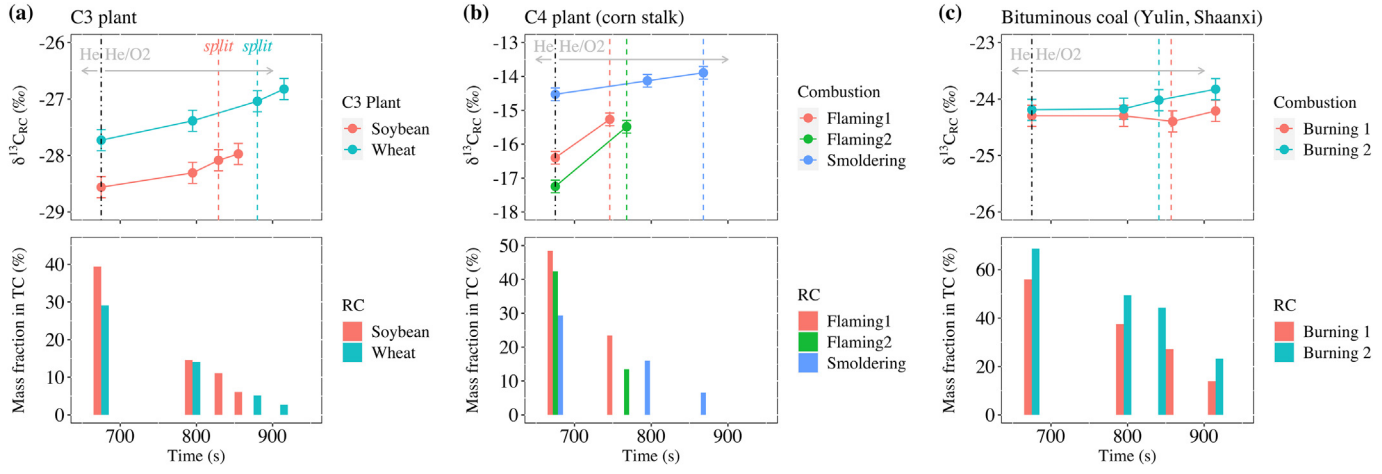

Fig. 4. The $\delta^{13}C$ values (symbols) and mass fractions (bars) of remaining carbon (RC) in TC. RC was captured at various times in He/O_2 phase (EUSAAR_2 protocol), after removal of desorbed OC in He phase. The carrier gas changing from He into He/O_2 is marked by the black dash-dot line. The OC/EC split time of each sample is marked by respective colored dashed lines. Thus, the RC trend represents the change from pOC/EC mixture to EC to partial EC, as pOC is gradually oxidized and finally EC is also combusted. The error bars represent the measurement uncertainty (0.19‰). (a) Two different C3 plants: soybean and wheat. (b) Three different combustion experiments of C4 plant (corn stalk): flaming and smoldering conditions. (c) Two different burning experiments of bituminous coal from Yulin City, Shaanxi Province, China.

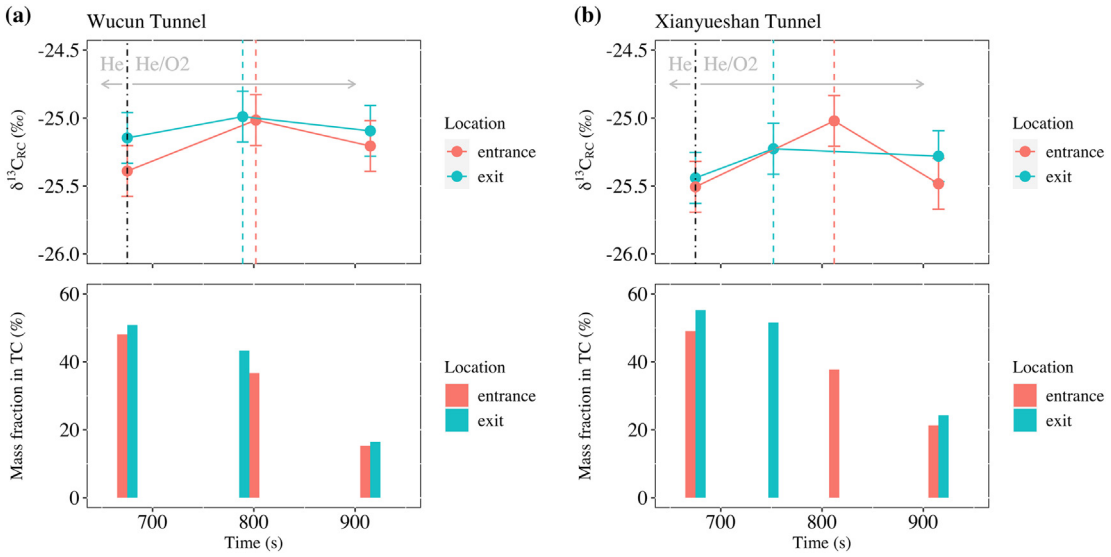

Fig. 5. The $\delta^{13}C$ values (symbols) and mass fractions (bars) of remaining carbon (RC) in TC for traffic emissions. RC is captured at various times after changing to the He/O_2 phase (EUSAAR_2 protocol). The carrier gas changing from He into He/O_2 is marked by the black dash-dot line. The OC/EC split time of each sample is marked by respective colored dashed lines. Thus, the RC trend represents the change from pOC/EC mixture to EC to partial EC, as pOC is gradually oxidized and finally EC is also combusted. The error bars represent the measurement uncertainty (0.19‰). (a) Entrance and exit of Wucun Tunnel. (b) Entrance and exit of Xianyueshan Tunnel. Both tunnels are in Xiamen City, China.

4. Discussion

The ^{13}C source signatures of EC are mainly dependent on the ^{13}C signatures of raw materials. Literature $\delta^{13}C$ values of various raw materials are summarized as histograms in Fig. 7, and given in more detail in Tables S1–S4. The ^{13}C signatures of different types of coal, C3 plants, and C4 plants follow approximately unimodal normal distributions. For crude oil, considering the geographical distribution (Fig. 6) together with the frequency distribution (Fig. 7), we separate ^{13}C signatures of crude oil into three groups. The three groups have different regional average $\delta^{13}C$ values: Group1, −26.0‰ to −27.5‰; Group2, −28.0‰ to −29.5‰; Group3, −30.0‰ to −31.0‰. Group1 is most enriched in ^{13}C and mainly located in low latitude areas, including the southern part of the USA, the Gulf of Mexico (coastline of North and South America), South Europe, the Middle East (Asia), the Gulf of Guinea (Africa), South and East Asia, and Oceania. Group2 has intermediate $\delta^{13}C$ values and is mainly located in mid-to-high latitude continental areas, including the north part of North America (Canada and north part of USA), Northwest Europe, North China, and the southern coastline of the Mediterranean Sea. Group3 is depleted in ^{13}C and located in high latitudes (around the Arctic Ocean), including Northeast Europe, North Asia (Russia), and the circum-Bering Strait area (Asian part, North American part).

The ^{13}C signatures of raw materials are usually different from the ^{13}C signatures of combustion products (e.g., TC, EC, OC) due to the isotope fractionation during combustion. For example, $\delta^{13}C$ values of TC or other burning residuals from traffic emissions are different from $\delta^{13}C$ of raw materials, with a difference of up to 2‰ comparing Fig. 7 and Table 3. The ^{13}C source signatures of EC can be further different from other carbon fractions of combustion emissions, including TC and OC

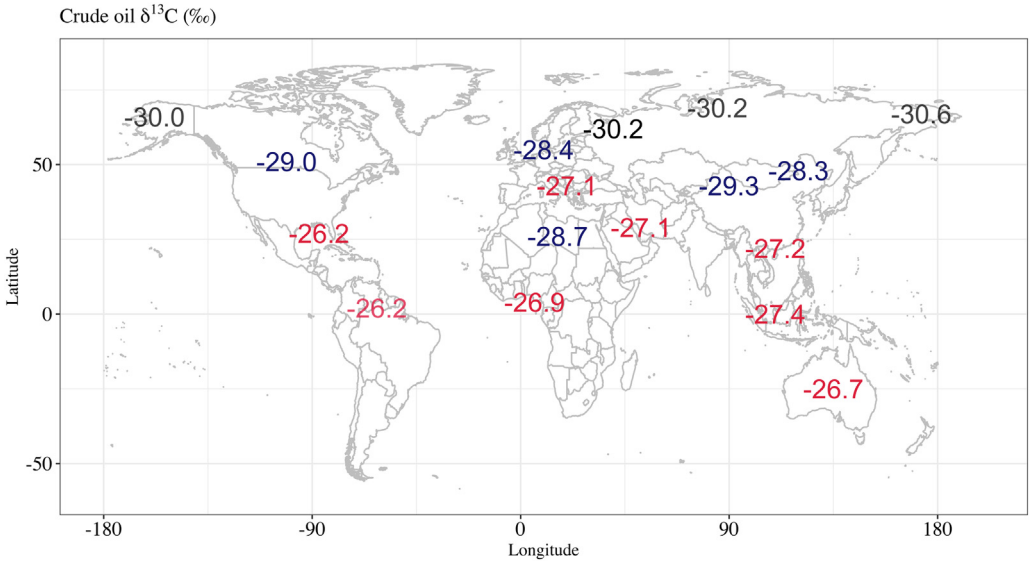

Fig. 6. The geographical distribution of crude oils with different ^{13}C signatures. The colors refer to different groups separated by regional average ^{13}C signatures, with red indicating $-26.0‰ < \delta^{13}C < -27.5‰$, blue $-28.0‰ < \delta^{13}C < -29.5‰$, black $-30.0‰ < \delta^{13}C < -31.0‰$.

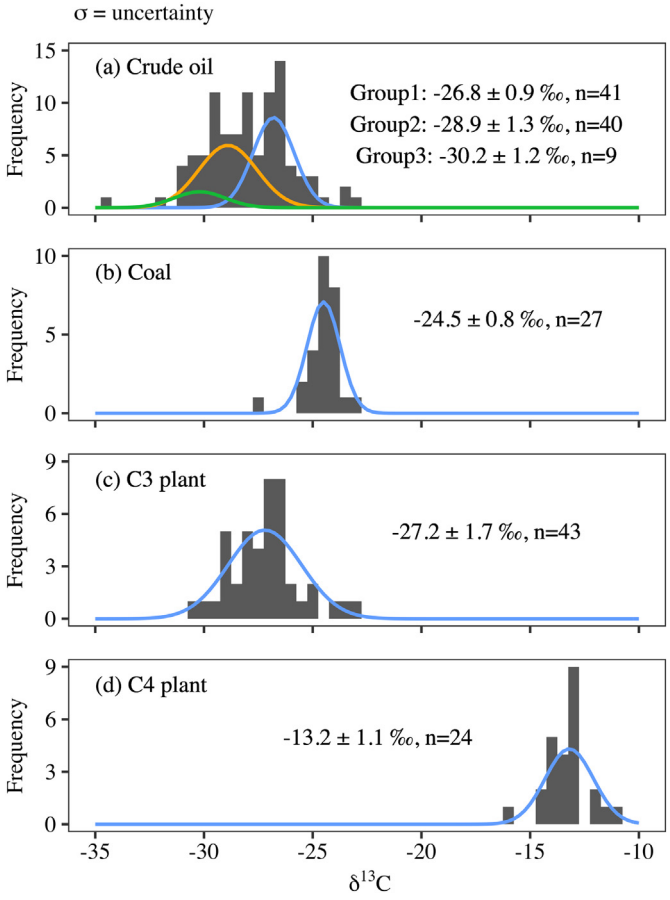

Fig. 7. Frequency distribution of ^{13}C signatures of raw materials reported in the literature (worldwide): (a) crude oil, (b) coal, (c) C3 plant, and (d) C4 plant. n is the number of studies. The data are presented in Tables S1–S4. See Section 4 for the description of three groups for crude oil.

(Sections 3.1–3.3). Therefore, using ^{13}C source signatures of raw materials or OC or TC to represent ^{13}C source signatures of EC for EC source apportionment is not recommended.

There are few studies reporting ^{13}C source signatures of EC, as summarized in Table 4. The ^{13}C source signatures of EC in the literature were determined by different EC isolation methods, and are thus potentially affected by pOC to a different extent. For all methods that desorb OC in He, some part of pOC may be classified as EC, as discussed in Sections 3.2 and 3.3. This is mitigated to a large extent by using an optical split point to isolate EC, but perfect physical separation of pOC from EC is impossible. If pOC is therefore significantly different in isotopic composition from EC, this can lead to biased values of $\delta^{13}C_{EC}$. This bias will vary with the method used and will be larger for methods that include all pOC to EC, such as the methods listed in Table 4 that remove OC in inert atmosphere. Results of these methods could be considered comparable to the data points at the start of the He/O_2 phase in Figs. 4 and 5. In addition, for methods using a low temperature during OC desorption in He, the most refractory OC fraction (e.g., OC desorbed at 650 °C step) might remain to be combusted together with EC. On the other hand, for methods that remove OC by heating the sample in an oxidizing atmosphere with long duration (e.g. CTO method), some part of EC can be lost in the OC removal step and only more refractory EC is actually captured for ^{13}C analysis (Han et al., 2007). This corresponds to data points after the split point in Figs. 4 and 5. These effects are considered in the following data selection to determine the ^{13}C source signatures of EC.

For coal combustion, the $\delta^{13}C_{RC}$ values do not change drastically before and after the OC/EC split time (within 0.5‰; Fig. 4), and this indicates that most EC isolation methods should give comparable results. For the combustion of C3 plants, increasing $\delta^{13}C_{RC}$ with analysis time indicate possible differences in $\delta^{13}C_{EC}$ values, obtained by different methods. Methods that desorb OC in inert atmosphere and do not use an optical split point, should yield lower $\delta^{13}C_{EC}$ values compared to thermal-optical method used in our work. On the other hand, methods using an oxidizing atmosphere to remove OC, and capture the most refractory part of EC should yield higher $\delta^{13}C$ values. However, since the difference over the whole analysis range is less than 1‰, different methods should only deviate moderately. This is an important result, since complete physical separation of pOC and EC is impossible, even for thermal-optical methods. Since $\delta^{13}C_{EC}$ of C3 plant and coal burning is not strongly influenced by OC/EC separation methods, the values in Table 4 together with the values analyzed in this study are summarized as ^{13}C source signatures of EC. This results in the recommended ^{13}C signatures of EC of −27.7‰ ± 1.1‰ for C3 plant burning and of −23.9‰ ± 0.8‰ for coal burning, respectively (Table 5, EC_worldwide).

The traffic $\delta^{13}C_{RC}$ values are relatively stable before and after the split-time in Fig. 5. Therefore, the traffic ^{13}C signatures of EC in Table 4 should not be strongly biased by the different EC isolation methods used. However, the ^{13}C signature are expected to vary with geographical location. The geographical distribution of traffic ^{13}C signatures of EC in Table 4 are highly related to the ^{13}C signatures of crude oil in Fig. 7. The most enriched ^{13}C signatures are found in Asia and South America, where crude oil in Group1 is used. In these regions, the averaged $\delta^{13}C_{EC}$ is −25.0‰ ± 0.6‰, which is more enriched compared to the ^{13}C signature of crude oil (−26.8‰ ± 0.9‰) in Group1. In Europe and North America, where the crude oils are representative for Group2, EC from traffic emissions is depleted in ^{13}C compared to EC associated with Group1. The $\delta^{13}C_{EC}$ of a tunnel study in Canada (−27.0‰ ± 0.5‰) (Huang et al., 2006), can be regarded as a typical ^{13}C signature of EC for these regions. This ^{13}C signature of EC is also enriched compared to the ^{13}C signature of crude oil (−28.9‰ ±

Table 3
^{13}C source signatures of TC and other burning residuals in the literature, reported as $\delta^{13}C$ (‰).

Continent	Location	C4 plant	C3 plant	Coal	Traffic	Fraction	References
Asia	China, Guangzhou				−24.6 to −25.5	TC; tunnel	(Dai et al., 2015)
	India		−25.9 to −29.4		−25.3 ± 0.3[a]	TC	(Agnihotri et al., 2011)
	Nepal				−25.51 to −26.05	TC; road aerosol	(Shakya et al., 2010)
Europe	France			−23.9 ± 0.5[a]	−26.5 ± 0.5[a]: diesel −26.0 ± 0.5[a]: fuel oil	TC; particle	(Widory et al., 2004)
	France			−23.5 to −25.5	−26.5 to −28.5	Burning residuals: Particles	(Widory, 2006)
North America	USA	−12.3 to −13.8 (±4)[b]	−24.6 to −26.1 (±0.7)[b]			Raw materials Ash	(Das et al., 2010)
Oceania	New Zealand				−24.7 to −28.3	TC	(Ancelet et al., 2011)
	New Zealand		−24.9 to −27.6			TC	(Ancelet et al., 2013)
Multiple			−25 to −32			TC	(Bird and Ascough, 2012)

[a] The standard deviation of several source samples.
[b] The isotope fractionation between raw materials and ash.

Table 4
^{13}C source signatures of EC determined by different thermal methods in the literature, reported as $\delta^{13}C$ (‰).

Continent	Location	C4 plant	C3 plant	Coal	Traffic	Steps to remove OC in the EC separation method	References
Asia	China, North	−14.88 ± 0.86	−27.77 ± 0.79	−24.68 ± 0.46		Thermal-optical	This study
	China, South				−25.11 ± 0.20	Thermal-optical	This study
	China	−13.62 ± 0.30[b]	−26.49 ± 1.17[a]	−23.46 ± 0.37[a]	−25.17 ± 0.40[a] Exhaust pipes	CTO-375: 375 °C, 24 h, air	(Chen et al., 2012)
	China, Shanghai		−25.04 to −27.11			340 °C, 3 h, O_2/N_2	(Wang et al., 2013)
	China	F: −15.0 to −22.2 S: −13.0 to −13.9[d]	−25.4 to −29.9			Smoke; 550/850 °C, 10 min each, He	(Liu et al., 2014)
	China, Nanjing	−19.3 ± 0.15[a]	−28.83 to −30.42	−22.17 to −26.15	−23.57 to −26.32 Exhaust pipes	550 °C, 15 min, He	(Guo et al., 2016)
	China, Hong Kong				−25.4 to −25.9 Urban aerosol[c]	375 °C, 3 h, inert	(Ho et al., 2006)
	Japan[e]	−16.1 to −19.3	−28 to −29.4	−23.3 ± 0.14[b]	−24.1 to −24.9 Tailpipes	550 °C, 15 min, He	(Kawashima and Haneishi, 2012)
Europe	Poland				Diesel: −28.3 Gasoline: −26.8	Soot	(Górka and Jędrysek, 2008)
North America	Canada				−26.47 to −27.47 Tunnel	Several steps (highest at 870 °C), He	(Huang et al., 2006)
South America	Brazil				−24.0 to −25.5 Tunnel	400 °C, He	(Tanner and Miguel, 1989)

[a] The standard deviation of several source samples.
[b] Uncertainty of ^{13}C measurement.
[c] Aerosols sampled at a road site in Hong Kong.
[d] F: flaming, S: smoldering.
[e] In this study, only rice plants, dry leaves, and soybean are selected, because some materials contribute little EC in real situations, such as potherb mustard, rosemary, chamomile, and watermelon. With the same reason, the sports-type vehicle which shows significantly enriched $\delta^{13}C$ (−20.6‰ ± 1.5‰) is excluded.

1.3‰) in Group2. However, one study may not be representative enough for Group2, so more studies are needed. The traffic $\delta^{13}C_{EC}$ in Poland (−26.8‰ to −28.3‰) (Górka and Jędrysek, 2008) is representative for Northeast Europe (including Russia) and is converted to −27.6 ± 0.8‰ for Group3. Again, this ^{13}C signature is enriched compared to the ^{13}C signature of crude oil (−30.2‰ ± 1.3‰) in these regions. In this study, we did not differentiate petrol and diesel due to limited studies. However, as a different fraction of crude oil, petrol seems to be slightly more enriched in ^{13}C than diesel (Tables 3–4 and Table S2).

More studies are needed to determine accurate traffic ^{13}C signatures of EC for specific locations, especially for Group2 and Group3 with limited studies. To determine local traffic ^{13}C signature of EC, we suggest tunnel studies with thermal-optical OC/EC separation to measure a representative mixture of the traffic fleet. The second-best option is to use the appropriate ^{13}C signature of EC according to the geographical region or the crude oil supply. Alternatively, with the known signature of the local crude oil, the average isotope fractionation from crude oil to traffic EC (1.8‰ ± 1.1‰, 2.0‰ ± 1.4‰, 2.6‰ ± 1.5‰, for three groups respectively) can be used for a rough estimate of $\delta^{13}C_{EC}$, as detailed in Supporting Information Section S7.

For C4 plant burning, the ^{13}C source signatures of EC vary in a wide range of −13.0‰ to −19.3‰ in Table 4, and are, in some instances, strongly depleted with respect to the ^{13}C signature of raw materials (−13.2‰ ± 1.1‰; Fig. 7). These depleted ^{13}C signatures of EC (Liu et al., 2014; Guo et al., 2016; Kawashima and Haneishi, 2012) could be caused by the strong isotope fractionation in the flaming condition of C4 plant burning, with significantly ^{13}C-depleted desorbed OC (Fig. 3b) and pOC (Fig. 4b). If pOC is not well separated, such as in the He-based thermal separation methods, the $\delta^{13}C_{EC}$ can be determined to be biased lower, especially for flaming combustion. Therefore, the thermal-optical OC/EC separation is important to determine the ^{13}C signature of EC for emissions from C4 plant burning. The thermal methods in the oxidizing atmosphere with long duration, such as CTO-375, can exclude pOC well, therefore the ^{13}C signature of EC reported in (Chen et al., 2012) is not strongly depleted. For smoldering combustion of C4 plant, the $\delta^{13}C_{OC}$ and $\delta^{13}C_{pOC}$ are relatively close to $\delta^{13}C_{EC}$ (Figs. 3b and 4b), so the smoldering ^{13}C signature of EC in (Liu et al., 2014) is

Table 5
Summarized worldwide and Chinese ^{13}C source signatures of EC and of raw materials.

	C4 plant $\delta^{13}C$ (‰)	Coal $\delta^{13}C$ (‰)	Traffic $\delta^{13}C$ (‰)	C3 plant $\delta^{13}C$ (‰)
Raw_materials_worldwide[a]	−13.2 ± 1.1	−24.5 ± 0.8	G1: −26.8 ± 0.9 G2: −28.9 ± 1.3 G3: −30.2 ± 1.2	−27.2 ± 1.7
EC_North_China[b]	−14.88 ± 0.86	−24.68 ± 0.46		−27.77 ± 0.79
EC_South_China[c]			−25.11 ± 0.20 (G1)	
EC_worldwide[d]	−14.0 ± 0.7	−23.9 ± 0.8	G1: −25.0 ± 0.6 G2: −27.0 ± 0.5 G3: −27.6 ± 0.8	−27.7 ± 1.1
Literature_A&H[e]	−16.4 ± 1.4**	−23.4 ± 1.3*	−25.5 ± 1.3*	−26.7 ± 1.8*

[a]Raw_materials_worldwide gives the averages of ^{13}C signatures of raw materials summarized in Fig. 7 and listed in Tables S1–S4. [b]EC_North_China and [c]EC_South_China are the ^{13}C source signatures of EC analyzed by thermal-optical method in this study. [d]EC_worldwide is the recommended ^{13}C signatures of EC if no local signature is available, and the values are averages of the selected values in Table 4 and this study. [e]Literature_A&H lists ^{13}C signatures complied in two previous studies (Andersson et al., 2015*; Ni et al., 2018**) for EC source apportionment, summarizing ^{13}C signatures of raw materials, TC, and EC together.

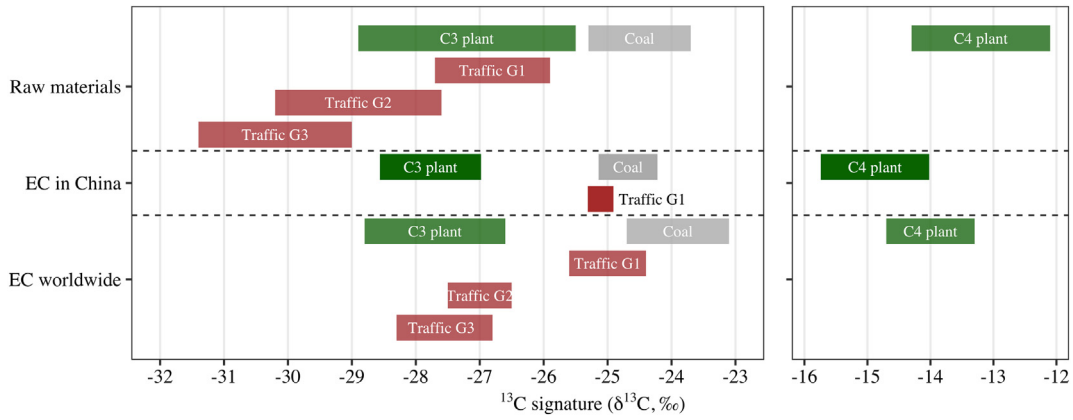

Fig. 8. Comparison of ^{13}C source signatures of raw materials and of EC in China and worldwide. The ^{13}C signature of EC of Traffic G1 in China refers to the traffic emissions in Xiamen City in South China, where crude oil is imported from the Middle East.

comparable to the source material and the values determined in this study. Taking pOC influence and isotope fractionation into consideration, $\delta^{13}C_{EC}$ of −13.62‰ ± 0.30‰ (Chen et al., 2012) and −13.0‰ to −13.9‰ (Liu et al., 2014) in Table 4 are selected and averaged with the value in this study to a composite $\delta^{13}C_{EC}$ for C4 plant burning, to be −14.0‰ ± 0.7‰ (Table 5, EC_worldwide).

The final recommended ^{13}C signatures and uncertainties of EC and of raw materials from the literature and this study are summarized in Table 5 and visualized in Fig. 8. The calculation of signatures and uncertainties are detailed in the Supporting Information Section S2. In summary, ^{13}C source signatures of EC are established for the main combustion sources, with EC from C3 and C4 plant burning slightly depleted in ^{13}C (0.5‰ and 0.8‰, respectively) compared to raw materials, while EC of coal combustion and traffic emissions enriched in ^{13}C (0.6‰ and 1.8‰, respectively).

5. Application case study

The ^{13}C source signatures of EC were applied to aerosol samples collected during clean and haze days in Xi'an, China, to illustrate the role of ^{13}C source signatures in the EC source apportionment using Bayesian MCMC approach (Section 2.3). As shown in Fig. 9, different ^{13}C source signatures of EC in Table 5 were taken for comparison, including EC_North_China (the North China ^{13}C signatures in Table 5, + traffic Group2), EC_worldwide (+ traffic Group2), and Literature_A&H (^{13}C signatures summarized in previous studies, combining raw material, TC, and EC). Using the North China ^{13}C signatures of EC, the resulting source apportionment shows 27% contribution of coal combustion and 47% contribution of traffic emissions to EC during clean days, and 35% (coal) vs 27% (traffic) during haze days, with the remaining contribution from C3 and C4 plant burning. Compared to EC_North_China, ^{13}C source signatures of EC_worldwide are more enriched for C4 plant burning and coal combustion by 0.8–0.9‰, and Literature_A&H are more depleted for C4 plant burning by 1.5‰ but more enriched for other three sources by as much as 1.1–1.5‰. Consequently, the different ^{13}C source signatures shift the estimated relative contribution of coal combustion and of traffic emissions, e.g., the coal contribution is underestimated by 6–11% if using the ^{13}C source signatures EC_worldwide relative to EC_North_China, and by 8–15% if using ^{13}C source signatures of Literature_A&H. Different ^{13}C source signatures lead to moderate changes in source contributions, but do not change the conclusion that the contribution of coal combustion increased and the contribution of traffic emissions decreased from clean to haze days.

To investigate if more precisely known source signatures improve source apportionment, the EC_North_China ^{13}C source signatures were used with different uncertainties (1σ and 2σ). This alters the median values (i.e., best estimate) and interquartile ranges (i.e., uncertainties) of the source contributions slightly in Fig. 9b. This indicates that narrower uncertainties of ^{13}C source signatures do not necessarily lead to lower uncertainties of source contributions, especially for source apportionment considering four sources.

Knowledge of the local sources is important. For example, the C4 plant burning should be considered in Xi'an, because it is used for heating and cooking in Xi'an and surrounding areas (Sun et al., 2017; Zhu et al., 2017). If C4 plant burning is ignored (source apportionment with only 3 sources in Fig. S4a), the results are significantly different

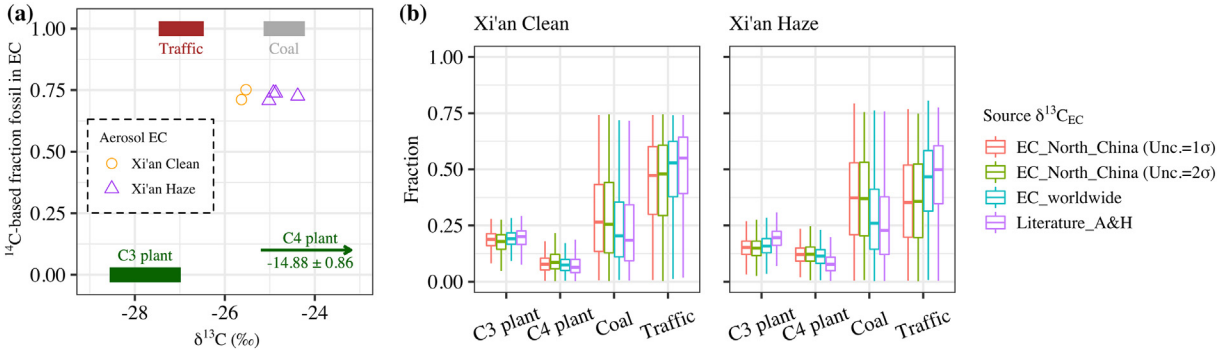

Fig. 9. (a) The ^{14}C-based fraction fossil vs. $\delta^{13}C$ for EC during haze and clean periods in Xi'an, China, with local ^{13}C signatures of EC, including C3 plant burning (green rectangle), traffic emissions (red rectangle), coal combustion (grey rectangle). ^{13}C source signatures of EC from C4 plant burning are also indicated ($\delta^{13}C = -14.88‰ \pm 0.86‰$). (b) The EC source apportionment results during clean and haze days, using different ^{13}C source signatures of EC and uncertainties in Table 5 in the Bayesian MCMC approach. The EC_North_China are the local ^{13}C signatures with different uncertainties (1σ: 68.27% of the distribution, 2σ: 95.45%). The data are presented in Table S13.

with overestimated contribution of coal combustion, because ^{13}C source signatures of C4 plant burning are strongly enriched compared to those of other sources. For 3-source apportionment, changing the uncertainties of ^{13}C source signatures (1σ and 2σ) can sometimes significantly shift the results (e.g., clean days in Fig. S4a). Therefore, the uncertainties of ^{13}C source signatures should also be carefully determined, considering the representativeness of local emission sources.

6. Conclusions

^{13}C signatures of EC were analyzed for typical combustion source samples from China using split point of the EUSAAR_2 protocol for separation of EC. The ^{13}C source signatures of EC were $-27.77‰ \pm 0.79‰$ ($\pm 1\sigma$) for C3 plant burning, $-14.88‰ \pm 0.86‰$ for C4 plant burning, $-24.68‰ \pm 0.46‰$ for coal combustion in North China, and $-25.11‰ \pm 0.20‰$ for traffic emissions in Xiamen City in South China, where crude oil is imported from the Middle East. The ^{13}C signatures of TC and OC fractions were also investigated and provided for reference.

For comparing the $\delta^{13}C_{EC}$ values obtained by different EC isolation methods, it is necessary to consider the influence of pOC, which forms due to pyrolysis during OC removal and can bias $\delta^{13}C_{EC}$, if not removed. Different methods separate pOC and EC to different extent. A sensitivity study shows that the influence of pOC on ^{13}C source signatures of EC is variable among the sources. For C3 plant burning, C4 plant smoldering, coal combustion, and traffic emissions, the biases are all within 1‰, even if pOC is not separated from EC at all or if EC is only partially recovered. Therefore, the ^{13}C signatures of EC based various EC isolation methods can be comparable. For flaming combustion of C4 plants, desorbed OC and pOC are significantly depleted in ^{13}C compared to raw plant materials, both in this study and in the literature. Biased ^{13}C signatures of EC (too depleted) are obtained, if pOC is not separated well from EC. The thermal-optical method for OC/EC separation seems successful in this, but also the CTO method gives comparable $\delta^{13}C_{EC}$ values. The ^{13}C source signatures from the literature obtained by the CTO method for both flaming and smoldering conditions and other methods only for smoldering conditions are therefore combined with the values obtained in this study (thermal-optical method) for the ^{13}C signature of EC of C4 plant burning. This results in a recommended value of $-14.0‰ \pm 0.7‰$ for $\delta^{13}C_{EC}$ from C4 plant burning.

For the other sources, selected $\delta^{13}C_{EC}$ values from the literature and the values in this study are summarized, resulting in $-27.7‰ \pm 1.1‰$ for C3 plant burning and $-23.9‰ \pm 0.8‰$ for coal combustion, representative of regions all around the globe. These are recommended for regions with local signatures unavailable. The traffic ^{13}C signatures of EC from the literature and from this study are highly correlated with the signatures of regional crude oils (but more enriched by around 2‰). Therefore, they are summarized in three groups: $-25.0‰ \pm 0.6‰$ for Group1 (low latitude), $-27.0‰ \pm 0.5‰$ for Group2 (mid-to-high latitude), and $-27.6‰ \pm 0.8‰$ for Group3 (high latitude). For more accurate and representative regional signatures, more studies on ^{13}C analysis of EC from combustion sources are needed, especially for traffic emissions.

CRediT authorship contribution statement

Peng Yao: Conceptualization, Methodology, Validation, Formal analysis, Investigation, Visualization, Data curation, Writing – original draft, Writing – review & editing. **Ru-Jin Huang:** Conceptualization, Validation, Investigation, Resources, Writing – review & editing, Supervision, Project administration, Funding acquisition. **Haiyan Ni:** Validation, Investigation, Resources, Visualization, Writing – review & editing. **Norbertas Kairys:** Validation, Investigation, Resources, Visualization, Writing – review & editing. **Lu Yang:** Investigation, Resources, Writing – review & editing. **Harro A.J. Meijer:** Validation, Investigation, Writing – review & editing. **Ulrike Dusek:** Conceptualization, Methodology, Validation, Investigation, Writing – review & editing, Supervision, Project administration, Funding acquisition.

Declaration of competing interest

The authors declare that they have no known competing financial interests or personal relationships that could have appeared to influence the work reported in this paper.

Acknowledgments

The authors acknowledge the project grants from the National Key Research and Development Program of China (grant no. 2017YFC0212701) and the program of China Scholarships Council No. 201806320346. Special thanks are given to Henk Jansen, Dipayan Paul, Marc Bleeker, Bert A.M. Kers, Marcel de Vries, and Roel A. Schellekens for their help with the TOA-IRMS modification and tests at CIO, and to Romke Tjoelker and Katrin Zenker for developing the system connection interface at CIO. Thanks to Matt Drury for the suggestions in the grammar and writing revision.

Appendix A. Supplementary data

Supporting Inforamtion to this article can be found online at https://doi.org/10.1016/j.scitotenv.2021.151284.

References

Agnihotri, R., Mandal, T.K., Karapurkar, S.G., Naja, M., Gadi, R., Ahammmed, Y.N., Kumar, A., Saud, T., Saxena, M., 2011. Stable carbon and nitrogen isotopic composition of bulk aerosols over India and northern Indian Ocean. Atmos. Environ. 45, 2828–2835. https://doi.org/10.1016/j.atmosenv.2011.03.003.

Aguilera, J., Whigham, L.D., 2018. Using the $^{13}C/^{12}C$ carbon isotope ratio to characterise the emission sources of airborne particulate matter: a review of literature. Isot. Environ. Health Stud. 54, 573–587. https://doi.org/10.1080/10256016.2018.1531854.

Ancelet, T., Davy, P.K., Trompetter, W.J., Markwitz, A., Weatherburn, D.C., 2011. Carbonaceous aerosols in an urban tunnel. Atmos. Environ. 45, 4463–4469. https://doi.org/10.1016/j.atmosenv.2011.05.032.

Ancelet, T., Davy, P.K., Trompetter, W.J., Markwitz, A., Weatherburn, D.C., 2013. Carbonaceous aerosols in a wood burning community in rural New Zealand. Atmos. Pollut. Res. 4, 245–249. https://doi.org/10.5094/APR.2013.026.

Andersson, A., Deng, J., Du, K., Zheng, M., Yan, C., Sköld, M., Gustafsson, Ö., 2015. Regionally-varying combustion sources of the January 2013 severe haze events over eastern China. Environ. Sci. Technol. 49, 2038–2043. https://doi.org/10.1021/es503855e.

Andrusevich, V.E., Engel, M.H., Zumberge, J.E., Brothers, L.A., 1998. Secular, episodic changes in stable carbon isotope composition of crude oils. Chem. Geol. 152, 59–72. https://doi.org/10.1016/S0009-2541(98)00096-5.

Bianchi, F., Kurtén, T., Riva, M., Mohr, C., Rissanen, M.P., Roldin, P., Berndt, T., Crounse, J.D., Wennberg, P.O., Mentel, T.F., Wildt, J., Junninen, H., Jokinen, T., Kulmala, M., Worsnop, D.R., Thornton, J.A., Donahue, N., Kjaergaard, H.G., Ehn, M., 2019. Highly oxygenated organic molecules (HOM) from gas-phase autoxidation involving peroxy radicals: a key contributor to atmospheric aerosol. Chem. Rev. 119, 3472–3509. https://doi.org/10.1021/acs.chemrev.8b00395.

Birch, M.E., Cary, R.A., 1996. Elemental carbon-based method for monitoring occupational exposures to particulate diesel exhaust. Aerosol Sci. Technol. 25, 221–241. https://doi.org/10.1080/02786829608965393.

Bird, M.I., Ascough, P.L., 2012. Isotopes in pyrogenic carbon: a review. Org. Geochem. 42, 1529–1539. https://doi.org/10.1016/j.orggeochem.2010.09.005.

Bond, T.C., Doherty, S.J., Fahey, D.W., Forster, P.M., Berntsen, T., DeAngelo, B.J., Flanner, M.G., Ghan, S., Kärcher, B., Koch, D., Kinne, S., Kondo, Y., Quinn, P.K., Sarofim, M.C., Schultz, M.G., Schulz, M., Venkataraman, C., Zhang, H., Zhang, S., Bellouin, N., Guttikunda, S.K., Hopke, P.K., Jacobson, M.Z., Kaiser, J.W., Klimont, Z., Lohmann, U., Schwarz, J.P., Shindell, D., Storelvmo, T., Warren, S.G., Zender, C.S., 2013. Bounding the role of black carbon in the climate system: a scientific assessment. J. Geophys. Res. Atmos. 118, 5380–5552. https://doi.org/10.1002/jgrd.50171.

Brand, W.A., Assonov, S.S., Coplen, T.B., 2010. Correction for the ^{17}O interference in $\delta(^{13}C)$ measurements when analyzing CO_2 with stable isotope mass spectrometry (IUPAC technical Report). Pure Appl. Chem. 82, 1719–1733. https://doi.org/10.1351/PAC-REP-09-01-05.

Cavalli, F., Viana, M., Yttri, K.E., Genberg, J., Putaud, J.-P., 2010. Toward a standardised thermal-optical protocol for measuring atmospheric organic and elemental carbon: the EUSAAR protocol. Atmos. Meas. Tech. 3, 79–89. https://doi.org/10.5194/amt-3-79-2010.

Chen, Y.-J., Cai, W.-W., Huang, G.-P., Li, J., Zhang, G., 2012. 33, 673–678.

Chen, B., Jie, D., Shi, M., Gao, P., Shen, Z., Uchida, M., Zhou, L., Liu, K., Hu, K., Kitagawa, H., 2015. Characteristics of ^{14}C and ^{13}C of carbonate aerosols in dust storm events in

China. Atmos. Res. 164–165, 297–303. https://doi.org/10.1016/j.atmosres.2015.06.003.
Chow, J.C., Watson, J.G., Crow, D., Lowenthal, D.H., Merrifield, T., 2001. Comparison of IMPROVE and NIOSH carbon measurements. Aerosol Sci. Technol. 34, 23–34. https://doi.org/10.1080/02786820119073.
Chung, C.E., Ramanathan, V., Decremer, D., 2012. Observationally constrained estimates of carbonaceous aerosol radiative forcing. Proc. Natl. Acad. Sci. 109, 11624–11629. https://doi.org/10.1073/pnas.1203707109.
Craig, H., 1957. Isotopic standards for carbon and oxygen and correction factors for mass-spectrometric analysis of carbon dioxide. Geochim. Cosmochim. Acta 12, 133–149. https://doi.org/10.1016/0016-7037(57)90024-8.
Dai, S., Bi, X., Chan, L.Y., He, J., Wang, B., Wang, X., Peng, P., Sheng, G., Fu, J., 2015. Chemical and stable carbon isotopic composition of $PM_{2.5}$ from on-road vehicle emissions in the PRD region and implications for vehicle emission control policy. Atmos. Chem. Phys. 15, 3097–3108. https://doi.org/10.5194/acp-15-3097-2015.
Das, O., Wang, Y., Hsieh, Y.-P., 2010. Chemical and carbon isotopic characteristics of ash and smoke derived from burning of C3 and C4 grasses. Org. Geochem. 41, 263–269. https://doi.org/10.1016/j.orggeochem.2009.11.001.
de Bello, F., Buchmann, N., Casals, P., Lepš, J., Sebastià, M.-T., 2009. Relating plant species and functional diversity to community $\delta^{13}C$ in NE Spain pastures. Agric. Ecosyst. Environ. 131, 303–307. https://doi.org/10.1016/j.agee.2009.02.002.
Dusek, U., ten Brink, H.M., Meijer, H.A.J., Kos, G., Mrozek, D., Röckmann, T., Holzinger, R., Weijers, E.P., 2013. The contribution of fossil sources to the organic aerosol in the Netherlands. Atmos. Environ. 74, 169–176. https://doi.org/10.1016/j.atmosenv.2013.03.015.
Dusek, U., Monaco, M., Prokopiou, M., Gongriep, F., Hitzenberger, R., Meijer, H.A.J., Röckmann, T., 2014. Evaluation of a two-step thermal method for separating organic and elemental carbon for radiocarbon analysis. Atmos. Meas. Tech. 7, 1943–1955. https://doi.org/10.5194/amt-7-1943-2014.
Dusek, U., Hitzenberger, R., Kasper-Giebl, A., Kistler, M., Meijer, H.A.J., Szidat, S., Wacker, L., Holzinger, R., Röckmann, T., 2017. Sources and formation mechanisms of carbonaceous aerosol at a regional background site in the Netherlands: insights from a year-long radiocarbon study. Atmos. Chem. Phys. 17, 3233–3251. https://doi.org/10.5194/acp-17-3233-2017.
Fang, W., Du, K., Andersson, A., Xing, Z., Cho, C., Kim, S.-W., Deng, J., Gustafsson, Ö., 2018. Dual-isotope constraints on seasonally resolved source fingerprinting of black carbon aerosols in sites of the four emission hot spot regions of China. J. Geophys. Res. Atmos. 123, 11735–11747. https://doi.org/10.1029/2018JD028607.
Farquhar, G., Richards, R., 1984. Isotopic composition of plant carbon correlates with water-use efficiency of wheat genotypes. Funct. Plant Biol. 11, 539. https://doi.org/10.1071/PP9840539.
Farquhar, G., O'Leary, M., Berry, J., 1982. On the relationship between carbon isotope discrimination and the intercellular carbon dioxide concentration in leaves. Funct. Plant Biol. 9, 121. https://doi.org/10.1071/PP9820121.
Fu, P.Q., Kawamura, K., Chen, J., Li, J., Sun, Y.L., Liu, Y., Tachibana, E., Aggarwal, S.G., Okuzawa, K., Tanimoto, H., Kanaya, Y., Wang, Z.F., 2012. Diurnal variations of organic molecular tracers and stable carbon isotopic composition in atmospheric aerosols over mt. Tai in the North China plain: an influence of biomass burning. Atmos. Chem. Phys. 12, 8359–8375. https://doi.org/10.5194/acp-12-8359-2012.
Gallagher, P.K., Johnson, D.W., 1973. The effects of sample size and heating rate on the kinetics of the thermal decomposition of $CaCO_3$. Thermochim. Acta 6, 67–83. https://doi.org/10.1016/0040-6031(73)80007-3.
Garbaras, A., Masalaite, A., Garbariene, I., Ceburnis, D., Krugly, E., Remeikis, V., Puida, E., Kvietkus, K., Martuzevicius, D., 2015. Stable carbon fractionation in size-segregated aerosol particles produced by controlled biomass burning. J. Aerosol Sci. 79, 86–96. https://doi.org/10.1016/j.jaerosci.2014.10.005.
GB/T 5751–2009, 2009. Chinese classification of coals (in Chinese).
Górka, M., Jędrysek, M.O., 2008. $\delta^{13}C$ of organic atmospheric dust deposited in Wrocław (SW Poland): critical remarks on the passive method. Geol. Q. 52, 115–126.
Guo, Z., Jiang, W., Chen, S., Sun, D., Shi, L., Zeng, G., Rui, M., 2016. Stable isotopic compositions of elemental carbon in $PM_{1.1}$ in north suburb of Nanjing Region, China. 168, 105–111. https://doi.org/10.1016/j.atmosres.2015.09.006.
Gustafsson, Ö., Haghseta, F., Chan, C., MacFarlane, J., Gschwend, P.M., 1997. Quantification of the dilute sedimentary soot phase: implications for PAH speciation and bioavailability. Environ. Sci. Technol. 31, 203–209. https://doi.org/10.1021/es960317s.
Gustafsson, Ö., Krusa, M., Zencak, Z., Sheesley, R.J., Granat, L., Engstrom, E., Praveen, P.S., Rao, P.S.P.P., Leck, C., Rodhe, H., 2009. Brown clouds over south asia: biomass or fossil fuel combustion? Science (80-.) 323, 495–498. https://doi.org/10.1126/science.1164857.
Hallquist, M., Wenger, J.C., Baltensperger, U., Rudich, Y., Simpson, D., Claeys, M., Dommen, J., Donahue, N.M., George, C., Goldstein, A.H., Hamilton, J.F., Herrmann, H., Hoffmann, T., Iinuma, Y., Jang, M., Jenkin, M.E., Jimenez, J.L., Kiendler-Scharr, A., Maenhaut, W., McFiggans, G., Mentel, T.F., Monod, A., Prévôt, A.S.H.H., Seinfeld, J.H., Surratt, J.D., Szmigielski, R., Wildt, J., 2009. The formation, properties and impact of secondary organic aerosol: current and emerging issues. Atmos. Chem. Phys. 9, 5155–5236. https://doi.org/10.5194/acp-9-5155-2009.
Han, Y., Cao, J., An, Z., Chow, J.C., Watson, J.G., Jin, Z., Fung, K., Liu, S., 2007. Evaluation of the thermal/optical reflectance method for quantification of elemental carbon in sediments. Chemosphere 69, 526–533. https://doi.org/10.1016/j.chemosphere.2007.03.035.
Heal, M.R., 2014. The application of carbon-14 analyses to the source apportionment of atmospheric carbonaceous particulate matter: a review. Anal. Bioanal. Chem. 406, 81–98. https://doi.org/10.1007/s00216-013-7404-1.
Heal, M.R., Naysmith, P., Cook, G.T., Xu, S., Duran, T.R., Harrison, R.M., 2011. Application of ^{14}C analyses to source apportionment of carbonaceous $PM_{2.5}$ in the UK. Atmos. Environ. 45, 2341–2348. https://doi.org/10.1016/j.atmosenv.2011.02.029.
Ho, K.F., Lee, S.C., Cao, J.J., Li, Y.S., Chow, J.C., Watson, J.G., Fung, K., 2006. Variability of organic and elemental carbon, water soluble organic carbon, and isotopes in Hong Kong. Atmos. Chem. Phys. 6, 4569–4576. https://doi.org/10.5194/acp-6-4569-2006.
Huang, B., Xiao, X., Zhang, M., 2003. Geochemistry, grouping and origins of crude oils in the Western Pearl River Mouth Basin, offshore South China Sea. Org. Geochem. 34, 993–1008. https://doi.org/10.1016/S0146-6380(03)00035-4.
Huang, L., Brook, J.R., Zhang, W., Li, S.M., Graham, L., Ernst, D., Chivulescu, A., Lu, G., 2006. Stable isotope measurements of carbon fractions (OC/EC) in airborne particulate: a new dimension for source characterization and apportionment. Atmos. Environ. 40, 2690–2705. https://doi.org/10.1016/j.atmosenv.2005.11.062.
Kawashima, H., Haneishi, Y., 2012. Effects of combustion emissions from the eurasian continent in winter on seasonal $\delta^{13}C$ of elemental carbon in aerosols in Japan. Atmos. Environ. 46, 568–579. https://doi.org/10.1016/j.atmosenv.2011.05.015.
Killelea, D.R., Campbell, V.L., Shuman, N.S., Utz, A.L., 2008. Isotope-selective chemical vapor deposition via vibrational activation. J. Phys. Chem. C 112, 9822–9827. https://doi.org/10.1021/jp801255q.
Laskin, A., Laskin, J., Nizkorodov, S.A., 2015. Chemistry of atmospheric Brown carbon. Chem. Rev. 115, 4335–4382. https://doi.org/10.1021/cr5006167.
Lewis, C.W., Klouda, G.A., Ellenson, W.D., 2004. Radiocarbon measurement of the biogenic contribution to summertime PM-2.5 ambient aerosol in Nashville,TN. 38, 6053–6061. https://doi.org/10.1016/j.atmosenv.2004.06.011.
Liu, G., Li, J., Xu, H., Wu, D., Liu, Y., Yang, H., 2014. Isotopic compositions of elemental carbon in smoke and ash derived from crop straw combustion. Atmos. Environ. 92, 303–308. https://doi.org/10.1016/j.atmosenv.2014.04.042.
López-Veneroni, D., 2009. The stable carbon isotope composition of $PM_{2.5}$ and PM_{10} in Mexico City metropolitan area air. Atmos. Environ. 43, 4491–4502. https://doi.org/10.1016/j.atmosenv.2009.06.036.
Malghani, S., Gleixner, G., Trumbore, S.E., 2013. Chars produced by slow pyrolysis and hydrothermal carbonization vary in carbon sequestration potential and greenhouse gases emissions. Soil Biol. Biochem. 62, 137–146. https://doi.org/10.1016/j.biortech.2007.11.042.
Masalaite, A., Holzinger, R., Ceburnis, D., Remeikis, V., Ulevičius, V., Röckmann, T., Dusek, U., 2018. Sources and atmospheric processing of size segregated aerosol particles revealed by stable carbon isotope ratios and chemical speciation. Environ. Pollut. 240, 286–296. https://doi.org/10.1016/j.envpol.2018.04.073.
Maslen, E., Grice, K., Métayer, P.Le, Dawson, D., Edwards, D., 2011. Stable carbon isotopic compositions of individual aromatic hydrocarbons as source and age indicators in oils from western australian basins. Org. Geochem. 42, 387–398. https://doi.org/10.1016/j.orggeochem.2011.02.005.
Mastalerz, M., Schimmelmann, A., 2002. Isotopically exchangeable organic hydrogen in coal relates to thermal maturity and maceral composition. Org. Geochem. 33, 921–931. https://doi.org/10.1016/S0146-6380(02)00064-5.
Mohn, J., Szidat, S., Fellner, J., Rechberger, H., Quartier, R., Buchmann, B., Emmenegger, L., 2008. Determination of biogenic and fossil CO_2 emitted by waste incineration based on $^{14}CO_2$ and mass balances. Bioresour. Technol. 99, 6471–6479. https://doi.org/10.1016/j.biortech.2007.11.042.
Moreno, T., Karanasiou, A., Amato, F., Lucarelli, F., Nava, S., Calzolai, G., Chiari, M., Coz, E., Artíñano, B., Lumbreras, J., Borge, R., Boldo, E., Linares, C., Alastuey, A., Querol, X., Gibbons, W., 2013. Daily and hourly sourcing of metallic and mineral dust in urban air contaminated by traffic and coal-burning emissions. Atmos. Environ. 68, 33–44. https://doi.org/10.1016/j.atmosenv.2012.11.037.
Morera-Gómez, Y., Cong, Z., Widory, D., 2021. Carbonaceous fractions contents and carbon stable isotope compositions of aerosols collected in the atmosphere of Montreal (Canada): seasonality, sources, and implications. Front. Environ. Sci. 9 (March), 1–18. https://doi.org/10.3389/fenvs.2021.622521.
Ni, H., Huang, R.-J., Cao, J., Liu, W., Zhang, T., Wang, M., Meijer, H.A.J., Dusek, U., 2018. Source apportionment of carbonaceous aerosols in Xi'an, China: insights from a full year of measurements of radiocarbon and the stable isotope ^{13}C. Atmos. Chem. Phys. 18, 16363–16383. https://doi.org/10.5194/acp-18-16363-2018.
Ni, H., Huang, R.-J., Cao, J., Dai, W., Zhou, J., Deng, H., Aerts-Bijma, A., Meijer, H.A.J., Dusek, U., 2019a. High contributions of fossil sources to more volatile organic aerosol. Atmos. Chem. Phys. 19, 10405–10422. https://doi.org/10.5194/acp-19-10405-2019.
Ni, H., Huang, R.-J., Cao, J., Guo, J., Deng, H., Dusek, U., 2019b. Sources and formation of carbonaceous aerosols in Xi'an, China: primary emissions and secondary formation constrained by radiocarbon. Atmos. Chem. Phys. 19, 15609–15628. https://doi.org/10.5194/acp-19-15609-2019.
Ni, H., Huang, R., Cosijn, M.M., Yang, L., Guo, J., Cao, J., Dusek, U., 2020. Measurement report: dual-carbon isotopic characterization of carbonaceous aerosol reveals different primary and secondary sources in Beijing and Xi'an during severe haze events. Atmos. Chem. Phys. 20, 16041–16053. https://doi.org/10.5194/acp-20-16041-2020.
O'Leary, M.H., 1988. Carbon isotopes in photosynthesis. Bioscience 38, 328–336. https://doi.org/10.2307/1310735.
Palstra, S.W.L., Meijer, H.A.J., 2014. Biogenic carbon fraction of biogas and natural gas fuel mixtures determined with ^{14}C. Radiocarbon 56, 7–28. https://doi.org/10.2458/56.16514.
Parnell, A.C., Inger, R., Bearhop, S., Jackson, A.L., 2010. Source partitioning using stable isotopes: coping with too much variation. PLoS One 5, e9672. https://doi.org/10.1371/journal.pone.0009672.
Pavuluri, C.M., Kawamura, K., 2012. Evidence for 13-carbon enrichment in oxalic acid via iron catalyzed photolysis in aqueous phase. Geophys. Res. Lett. 39, n/a-n/a. https://doi.org/10.1029/2011GL050398.
Pöschl, U., 2005. Atmospheric aerosols: composition, transformation, climate and health effects. Angew. Chemie Int. Ed. 44, 7520–7540. https://doi.org/10.1002/anie.200501122.
Ramanathan, V., Carmichael, G., 2008. Global and regional climate changes due to black carbon. Nat. Geosci. 1, 221–227. https://doi.org/10.1038/ngeo156.

Ren, S.-J., Yu, G.-R., 2011. Carbon isotope composition ($\delta^{13}C$) of C3 plants and water use efficiency in China. Chin. J. Plant Ecol. 35, 119–124. https://doi.org/10.3724/SP.J.1258.2011.00119.

Schimmelmann, A., Qi, H., Coplen, T.B., Brand, W.A., Fong, J., Meier-Augenstein, W., Kemp, H.F., Toman, B., Ackermann, A., Assonov, S., Aerts-Bijma, A.T., Brejcha, R., Chikaraishi, Y., Darwish, T., Elsner, M., Gehre, M., Geilmann, H., Gröning, M., Hélie, J.-F., Herrero-Martín, S., Meijer, H.A.J., Sauer, P.E., Sessions, A.L., Werner, R.A., 2016. Organic reference materials for hydrogen, carbon, and nitrogen stable isotope-ratio measurements: caffeines, n-alkanes, fatty acid methyl esters, glycines, l-valines, polyethylenes, and oils. Anal. Chem. 88, 4294–4302. https://doi.org/10.1021/acs.analchem.5b04392.

Schumacher, M., Werner, R.A., Meijer, H.A.J., Jansen, H.G., Brand, W.A., Geilmann, H., Neubert, R.E.M., 2011. Oxygen isotopic signature of CO_2 from combustion processes. Atmos. Chem. Phys. 11, 1473–1490. https://doi.org/10.5194/acp-11-1473-2011.

Shakya, K.M., Ziemba, L.D., Griffin, R.J., 2010. Characteristics and sources of carbonaceous, ionic, and isotopic species of wintertime atmospheric aerosols in Kathmandu valley, Nepal. 10, 219–230. https://doi.org/10.4209/aaqr.2009.10.0068.

Sun, J., Shen, Z., Cao, J., Zhang, L., Wu, T., Zhang, Q., Yin, X., Lei, Y., Huang, Y., Huang, R.-J., Liu, S., Han, Y., Xu, H., Zheng, C., Liu, P., 2017. Particulate matters emitted from maize straw burning for winter heating in rural areas in guanzhong plain, China: current emission and future reduction. Atmos. Res. 184, 66–76. https://doi.org/10.1016/j.atmosres.2016.10.006.

Suto, N., Kawashima, H., 2016. Global mapping of carbon isotope ratios in coal. J. Geochem. Explor. 167, 12–19. https://doi.org/10.1016/j.gexplo.2016.05.001.

Szidat, S., Jenk, T., Gäggeler, H., Synal, H.-A., Fisseha, R., Baltensperger, U., Kalberer, M., Samburova, V., Reimann, S., Kasper-Giebl, A., Hajdas, I., 2004a. Radiocarbon (^{14}C)-deduced biogenic and anthropogenic contributions to organic carbon (OC) of urban aerosols from Zürich,Switzerland. 38, 4035–4044. https://doi.org/10.1016/j.atmosenv.2004.03.066.

Szidat, S., Jenk, T.M., Gäggeler, H.W., Synal, H.-A., Hajdas, I., Bonani, G., Saurer, M., 2004b. THEODORE, a two-step heating system for the EC/OC determination of radiocarbon (^{14}C) in the environment. 223–224, 829–836. https://doi.org/10.1016/j.nimb.2004.04.153.

Tanner, R.L., Miguel, A.H., 1989. Carbonaceous aerosol sources in Rio de Janeiro. Aerosol Sci. Technol. 10, 213–223. https://doi.org/10.1080/02786828908959236.

Turekian, V.C., Macko, S., Ballentine, D., Swap, R.J., Garstang, M., 1998. Causes of bulk carbon and nitrogen isotopic fractionations in the products of vegetation burns: laboratory studies. Chem. Geol. 152, 181–192. https://doi.org/10.1016/S0009-2541(98)00105-3.

Turney, C.S.M., Wheeler, D., Chivas, A.R., 2006. Carbon isotope fractionation in wood during carbonization. Geochim. Cosmochim. Acta 70, 960–964. https://doi.org/10.1016/j.gca.2005.10.031.

Wang, G., Yao, J., Zeng, Y., Huang, Y., Qian, Y., Liu, W., Li, Y., Yuan, N., Liu, S., Shan, J., 2013. Source apportionment of carbonaceous particulate matter in a Shanghai suburb based on carbon isotope composition. Aerosol Sci. Technol. 47, 239–248. https://doi.org/10.1080/02786826.2012.743959.

Weiguo, L., Xiahong, F., Youfeng, N., Qingle, Z., Yunning, C., Zhisheng, A.N., 2005. $\delta^{13}C$ variation of C3 and C4 plants across an asian monsoon rainfall gradient in arid northwestern China. Glob. Chang. Biol. 11, 1094–1100. https://doi.org/10.1111/j.1365-2486.2005.00969.x.

Widory, D., 2006. Combustibles, fuels and their combustion products: a view through carbon isotopes. Combust. Theor. Model. 10, 831–841. https://doi.org/10.1080/13647830600720264.

Widory, D., Roy, S., Le Moullec, Y., Goupil, G., Cocherie, A., Guerrot, C., 2004. The origin of atmospheric particles in Paris: a view through carbon and lead isotopes. Atmos. Environ. 38, 953–961. https://doi.org/10.1016/j.atmosenv.2003.11.001.

Yang, Q., Li, X., Liu, W., Zhou, X., Zhao, K., Sun, N., 2011. Carbon isotope fractionation during low temperature carbonization of foxtail and common millets. Org. Geochem. 42, 713–719. https://doi.org/10.1016/j.orggeochem.2011.06.012.

Yang, S., Ding, Z., Wang, X., Tang, Z., Gu, Z., 2012. Negative $\delta^{18}O$–$\delta^{13}C$ relationship of pedogenic carbonate from northern China indicates a strong response of C3/C4 biomass to the seasonality of Asian monsoon precipitation. Palaeogeogr. Palaeoclimatol. Palaeoecol. 317–318, 32–40. https://doi.org/10.1016/j.palaeo.2011.12.007.

Yao, P., Ni, H., Paul, D., Masalaite, A., Huang, R.-J., Meijer, H.A.J., Dusek, U., 2021. An automated method for thermal-optical separation of aerosol organic/elemental carbon for ^{13}C analysis at the sub-μgC level: a comprehensive assessment. Sci. Total Environ. 100, 150031. https://doi.org/10.1016/j.scitotenv.2021.150031.

Zenker, K., Vonwiller, M., Szidat, S., Calzolai, G., Giannoni, M., Bernardoni, V., Jedynska, A., Henzing, B., Meijer, H.A.J., Dusek, U., 2017. Evaluation and inter-comparison of oxygen-based OC-EC separation methods for radiocarbon analysis of ambient aerosol particle samples. Atmosphere (Basel) 8, 226. https://doi.org/10.3390/atmos8110226.

Zenker, K., Sirignano, C., Riccio, A., Chianese, E., Calfapietra, C., Prati, M.V., Masalaite, A., Remeikis, V., Mook, E., Meijer, H.A.J., Dusek, U., 2020. $\delta^{13}C$ signatures of organic aerosols: measurement method evaluation and application in a source study. J. Aerosol Sci. 145, 105534. https://doi.org/10.1016/j.jaerosci.2020.105534.

Zhang, Y.L., Perron, N., Ciobanu, V.G., Zotter, P., Minguillón, M.C., Wacker, L., Prévôt, A.S.H., Baltensperger, U., Szidat, S., 2012. On the isolation of OC and EC and the optimal strategy of radiocarbon-based source apportionment of carbonaceous aerosols. Atmos. Chem. Phys. 12, 10841–10856. https://doi.org/10.5194/acp-12-10841-2012.

Zhang, Y., Cai, J., Wang, S., He, K., Zheng, M., 2017. Review of receptor-based source apportionment research of fine particulate matter and its challenges in China. Sci. Total Environ. 586, 917–929. https://doi.org/10.1016/j.scitotenv.2017.02.071.

Zheng, S.X., Shangguan, Z.P., 2007. Foliar $\delta^{13}C$ values of nine dominant species in the loess plateau of China. Photosynthetica 45, 110–119. https://doi.org/10.1007/s11099-007-0017-1.

Zhu, C.-S., Cao, J.-J., Tsai, C.-J., Zhang, Z.-S., Tao, J., 2017. Biomass burning tracers in rural and urban ultrafine particles in Xi'an, China. 8, 614–618. https://doi.org/10.1016/j.apr.2016.12.011.